

Improving triplet excited-state absorption and lifetime of cationic iridium (III) complexes by extending π -conjugation of the 2-(2-quinoliny) quinoxaline ligand

Hui Li, Shan Liu, Levi Lystrom, Svetlana Kilina, Wenfang Sun*

Department of Chemistry and Biochemistry, North Dakota State University, Fargo, ND, 58108-6050, USA

ARTICLE INFO

Keywords:

Iridium(III) complex
Photophysical property
Long triplet lifetime
Excited-state absorption
Reverse saturable absorption

ABSTRACT

The synthesis and photophysical properties (UV-vis absorption, emission, and transient absorption) of four cationic Ir(III) complexes ($C^*N)_2Ir(R-quqo)^+$ (HC^*N = 1-phenylisoquinoline (**piq**) and 1,2-diphenylpyreno[4,5-*d*]imidazole (**dppi**), **quqo** = 2-(2-quinoliny)quinoxaline, **R** = H or fluorenyl) are reported. The UV-vis absorption and emission were simulated by time-dependent density functional theory (TDDFT). Influences of extending π -conjugation of the C^*N ligand and the diimine ligand on the singlet and triplet excited-state absorption and lifetimes of these complexes were explored. All complexes exhibited intense ligand-localized $^1\pi,\pi$ transitions, broad and structureless metal-to-ligand charge transfer (1MLCT) / ligand-to-ligand charge transfer (1LLCT) transitions, and very weak spin-forbidden $^3MLCT/{}^3LLCT/{}^3\pi,\pi$ transitions in their UV-vis absorption spectra. The two complexes that bear fluorenyl-substituted **quqo** ligands (**Ir-3** and **Ir-4**) also possessed a broad intraligand charge transfer (1ILCT) / $^1\pi,\pi$ band at 430–550 nm. The predominant $^3ILCT/{}^3\pi,\pi$ characters of the triplet excited states of **Ir-3** and **Ir-4** improved their phosphorescent emission quantum yields and prolonged their triplet lifetimes compared to the weaker and short-lived emission of **Ir-1** and **Ir-2**. In contrast to the very weak nanosecond transient absorption (TA) of **Ir-1** and **Ir-2**, **Ir-3** and **Ir-4** possessed much stronger TA signals at 520–800 nm upon nanosecond laser excitation. These complexes exhibited moderate to strong reverse saturable absorption (RSA) at 532 nm for ns laser pulses, with the RSA trend following **Ir-1** > **Ir-2** \approx **Ir-3** > **Ir-4**. Considering the long triplet excited-state lifetimes and broadband TA, complexes **Ir-3** and **Ir-4** could be potential broadband RSA materials.

1. Introduction

In the past a few decades, cyclometalated Ir(III) complexes have attracted growing interests due to their potential applications in organic light-emitting diodes (OLEDs) [1–5], light-emitting electrochemical cells (LEECs) [6,7], photocatalysis [2,8,9], luminescent biological labeling and cellular imaging [10–13], chemo- and biosensing [14,15], photodynamic therapy [11,16], and nonlinear optics [17–20], etc [21]. More recently, Ir(III) complexes, especially the monocationic complexes, have been investigated as reverse saturable absorbers for optical limiting applications because of their broad and strong excited-state absorption [22–40]. Part of the interest in investigating the Ir(III) complexes as reverse saturable absorbers lies in the fact that the ground- and excited-state properties of the Ir(III) complexes can be readily tuned via modifications of the diimine and/or cyclometalating ligands with different substituents and/or π -conjugation [22–44]. More

notably, the major absorption bands of most of the Ir(III) complexes studied are below 400 nm, which makes them almost transparent in the visible to the near-IR region. This feature is crucial for reverse saturable absorbers that require a low loss in the visible to the near-IR region [22–40].

Reverse saturable absorption (RSA) is one of the nonlinear absorption phenomena in which the excited state absorbs strongly than the ground state, resulting in decreased transmission when the incident fluence increases. RSA can be used in optical limiting [22–40], optical switching [45], laser mode-locking [46], optical pulse compressing [47], etc. According to the RSA mechanism [22–40,48], ground-state molecules are first excited to the lowest singlet excited state (S_1) via one-photon absorption, then the excited molecules decay to the lowest triplet excited state (T_1) via intersystem crossing (ISC). For heavy-atom containing molecules, such as Ir(III) complexes, the ISC time is much shorter than the ns laser pulse duration, RSA of ns laser pulses primarily

* Corresponding author.

E-mail address: Wenfang.Sun@ndsu.edu (W. Sun).

<https://doi.org/10.1016/j.jphotochem.2020.112609>

Received 19 February 2020; Received in revised form 1 May 2020; Accepted 2 May 2020

Available online 20 May 2020

1010-6030/© 2020 Elsevier B.V. All rights reserved.

occurs via the triplet excited-state absorption [24]. Therefore, Ir(III) complexes with higher triplet quantum yields and long-lived triplet excited states are specially interesting.

For monocationic Ir(III) complexes, the nature and energy of their lowest triplet excited state can be readily altered by an appropriate choice and modification of the diimine and/or cyclometalating ligands [22–44,49–52], which is a favorable feature in developing ideal RSA materials. It has been reported that different diimine ligands significantly impacted the triplet excited state quantum yield and lifetime for the Ir(III) complexes [25,53]. When the electronic nature of the substituent on the diimine and/or cyclometalating ligand changed, or the number, or position of the substitutes varied, the impacts on the lowest triplet excited state of Ir(III) complexes became more salient [27,30,35,54–56]. In addition, extending the π -conjugation via benzannulation on the diimine and/or the cyclometalating ligand or introducing π -conjugated substituent on these ligands can adjust the nature of the triplet excited state and thus impact the triplet excited-state absorption and lifetime of Ir(III) complexes drastically [22–26,29,32–34,36–40,57].

Our group previously reported that the triplet lifetimes of the monocationic cyclometalating Ir(III) complexes could be extended upon benzannulation at certain positions of the cyclometalating ligand via switching the lowest triplet excited state (T_1) to the cyclometalating ligand-localized $^3\pi,\pi^*$ state when the diimine ligand has limited π -conjugation [24,40]. Alternatively, incorporation of a π -conjugated motif, such as benzothiazolylfluoren-2-yl (BTF), to the diimine ligand (such as 2,2'-bipyridine (bpy) or phenanthroline (phen)) also increased the T_1 lifetime of the Ir(III) complexes due to the nature of the T_1 state being altered to the diimine ligand-localized $^3\text{ILCT}/^3\pi,\pi^*$ state [23,26]. In contrast, benzannulation at certain positions of the diimine and/or cyclometalating ligand significantly shortened the T_1 lifetime although such a benzannulation red-shifted the lowest-energy absorption band in the UV–vis absorption spectra of the Ir(III) complexes [25,34,38–40,57,58].

The aforementioned π -conjugation or substituent effects on the lifetimes of the T_1 states in Ir(III) complexes intrinsically arise from the overplay of the $^3\text{MLCT}/^3\text{LLCT}$ and $^3\pi,\pi$ characters. The more the $^3\pi,\pi$ character, the longer the T_1 lifetime. On the other hand, the $^1\text{MLCT}/^1\text{LLCT}$ transition energy that is directly related to the energy gap between the diimine ligand based LUMO (lowest unoccupied molecular orbital) and the d-orbital and cyclometalating ligand based HOMO (highest occupied molecular orbital), determines the lowest-energy absorption band(s) in the UV–vis absorption spectra of the Ir(III) complexes. We have demonstrated that benzannulation of bpy or 2-phenylpyridine (ppy) ligand at an appropriate site of the ligands could red-shift the $^1,^3\text{CT}$ (charge transfer) absorption band in the monocationic Ir(III) complexes, accompanied by a reduced T_1 lifetime due to increased nonradiative decay rates [25,34,38–40,57,58]. Such dual effects were exemplified in the 2-(2-quinolinyl)quinoxaline (**quqo**) containing Ir(III) complexes [34]: on one hand, the $^1,^3\text{CT}$ absorption band was red-shifted to 730 nm due to the strong electron-withdrawing ability and expansive π -conjugation of the **quqo** ligand; on the other hand, the T_1 lifetime (ps range) was too short to allow the ns transient absorption (TA) to be detected. Although modification of the ppy ligand by attaching the BTF motif at the different positions of the ppy ligand slightly prolonged the T_1 lifetime, the triplet TA was still difficult to be monitored [34].

For developing Ir(III) complexes with broadband RSA, red-shifting the weak $^1,^3\text{CT}$ absorption band while maintaining long-lived T_1 state is critical. To realize this goal, we synthesized four monocationic Ir(III) complexes bearing **quqo** as the diimine ligand (see Chart 1). Two strategies aiming at improving the triplet lifetimes of these complexes were adopted in designing these complexes. First, 1-phenylisoquinoline (**piq**) and 1,2-diphenylpyreno[4,5-*d*]imidazole (**dppi**), which possess different degrees of π -conjugation, were chosen as the cyclometalating C^N ligand. We expected to switch the T_1 state character from the

$^3\text{MLCT}/^3\text{LLCT}$ configuration to the predominant C^N ligand-centered $^3\pi,\pi^*$ configuration via benzannulation and thus increase the T_1 lifetime [24,36,40]. Secondly, building donor-acceptor-donor (D-A-D) character in the diimine ligand by linking two π -donating fluorene substituents to the electron-deficient **quqo** ligand would incorporate $^3\text{ILCT}$ character into the T_1 state in addition to extending the π -conjugation of the diimine ligand. Both effects have been manifested to prolong the T_1 lifetime from our previous studies [23,26,33,36,37]. Although the synthesis and some photophysical properties of **Ir-1** was reported in earlier literature [57], its RSA was investigated here for the first time. **Ir-1** was also used for comparison purpose to better understand the π -conjugation effects in the other three new complexes.

2. Experimental section

2.1. Materials and methods

All chemicals and reagents (analytical grade) for synthesis were purchased from commercial sources and used as received unless otherwise noted. Tetrahydrofuran was distilled over sodium/benzophenone under the nitrogen atmosphere prior to use. The solvents used for photophysical experiments were spectroscopic grade and obtained from VWR International and used as is without further purification. 1-Phenylisoquinoline (**piq**) was purchased from Aldrich Chemical Co.

The synthetic schemes for ligand **L** and the Ir(III) complexes are displayed in Scheme 1. The precursors 6-amino-2-methylquinoxaline [59,60] and **F8-B** [61], the cyclometalating ligand **dppi** [62–64] and its corresponding chloro-bridged Ir(III) dimer **[Ir(dppi)₂Cl]₂** [24], and the **piq** Ir(III) dimer **[Ir(piq)₂Cl]₂** [65] were synthesized according to the literature procedures. The synthetic details and characterization data for ligand **L** and the Ir(III) complexes are provided below. ^1H NMR spectra were recorded on a Varian Oxford-400 or Varian Oxford-500 spectrometer in CDCl_3 or d_6 -DMSO with tetramethylsilane (TMS) as the internal standard. High resolution mass (HRMS) analyses were performed on a Waters Synapt G2-Si high resolution mass spectrometer. Elemental analyses were conducted by NuMega Resonance Laboratories, Inc. in San Diego, CA.

2.1.1. Synthesis of ligand **L**

The synthetic procedure for the starting compound **1** is provided in the Supporting Information.

Compound **2**. At $-2 \sim -5^\circ\text{C}$, 6-amino-2-methylquinoxaline (0.08 g, 0.5 mmol) was added into a mixture of 48% HBr (0.56 mL), 85% H_3PO_4 (0.18 mL) and H_2O (0.37 mL), and stirred for 20 min. A solution of sodium nitrite (0.069 g, 1.0 mmol) in 0.43 mL H_2O was added dropwise. The reaction mixture was stirred for an additional 0.5 h at $-2 \sim -5^\circ\text{C}$, and a solution of CuBr (0.107 g, 0.75 mmol) in 0.32 mL 48% HBr was added dropwise. The reaction mixture was stirred for 30 min at $-2 \sim -5^\circ\text{C}$ and then stirred at r.t. for 3 h until no more gas evolution was observed. The reaction mixture was basified to pH = 8 with a saturated aqueous Na_2CO_3 solution and extracted with CH_2Cl_2 . The combined organic layers were washed with 5% aqueous NaHSO_3 , and then the mixture was dried over anhydrous Na_2SO_4 . After removal of the solvent, the residue was purified by column chromatography (silica gel, *n*-hexane/ethyl acetate = 20/1, v/v) to give 36 mg white solid (yield: 32%). ^1H NMR (400 MHz, CDCl_3): δ 8.73 (s, 1 H), 8.25 (d, J = 2.0 Hz, 1 H), 7.88 (d, J = 8.8 Hz, 1 H), 7.81 (dd, J = 8.8, 2.0 Hz, 1 H), 2.76 (s, 3 H).

Compound **3**. To a solution of 6-bromo-2-methylquinoxaline (1.43 g, 6.14 mmol) in 60 mL pyridine, SeO_2 (1.50 g, 13.51 mmol) was added. Then the reaction mixture was heated to 100°C for 16 h. After cooling to r.t., the mixture was filtered, and the filtrate was concentrated. The residue was poured into saturated NaHCO_3 aqueous solution, and then filtered to remove the insoluble part. Floccule precipitates were formed after adding dilute HCl aq. (15%, wt.) in the filtrate. After filtration and drying, 1.55 g white solid was obtained as

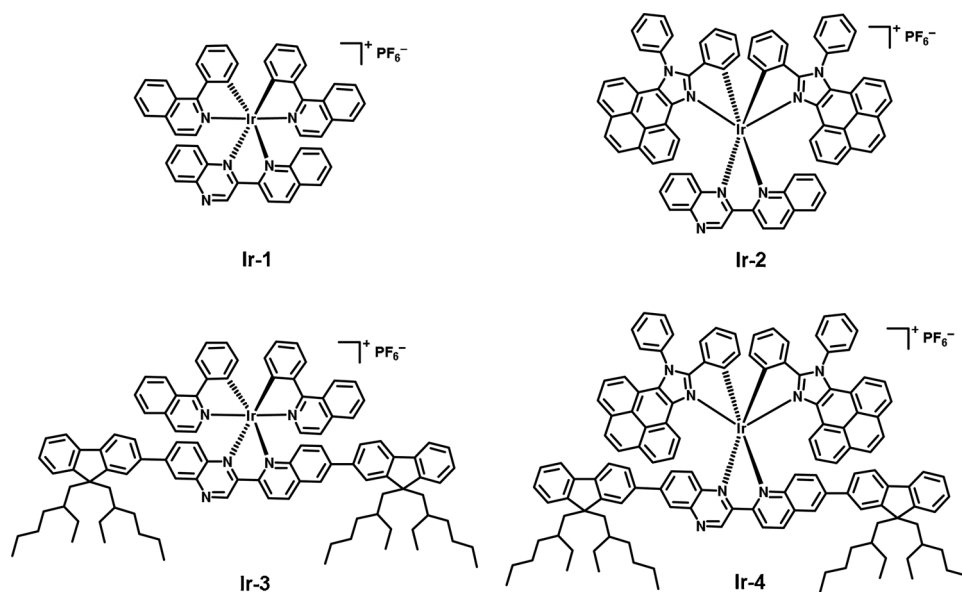


Chart 1. Chemical structures of Ir(III) complexes Ir-1 – Ir-4.

compound **3** (yield: 79%). ^1H NMR (400 MHz, $\text{DMSO}-d_6$): δ 9.38 (s, 1 H), 8.36 (d, $J = 1.6$ Hz, 1 H), 8.16 (d, $J = 8.4$ Hz, 1 H), 8.03 (dd, $J = 8.8$, 2.0 Hz, 1 H).

Compound **4**. In 60 mL DMF, compound **3** (1.55 g, 6.13 mmol), triethylamine (8 mL), *N,O*-dimethylhydroxylamine hydrochloride (0.72 g, 7.35 mmol), and HBTU (2.70 g, 7.35 mmol) were added, and the mixture was stirred for 24 h at r.t. The reaction mixture was diluted with ethyl acetate and washed with NaHCO_3 aq. solution and water, respectively. Then the mixture was dried over anhydrous Na_2SO_4 and the solvent was removed to give a crude product. The crude product was purified by column chromatography on silica gel with *n*-hexane/ethyl acetate = 5/1 (v/v) to give 1.56 g white solid (yield: 86%). ^1H NMR (400 MHz, CDCl_3): δ 9.10 (s, 1 H), 8.34 (d, $J = 2.4$ Hz, 1 H), 8.01 (d, $J = 8.8$ Hz, 1 H), 7.90 (dd, $J = 8.8$, 2.4 Hz, 1 H), 3.79 (s, 3 H), 3.47 (s, 3 H).

Compound **5**. To a solution of compound **4** (0.59 g, 2.0 mmol) in dry THF (40 mL), methylmagnesium bromide (0.733 mL, 2.2 mmol, 3 M in ether) was added at -78°C and reacted for 1 h. Then the reaction was quenched with saturated ammonium chloride aq. solution. After stirring for 30 min at r.t., the product was extracted with ethyl acetate and washed with H_2O . The organic phase was dried over anhydrous Na_2SO_4 and filtrated. The volatile was removed under reduced pressure. The residue was then purified by silica gel column chromatography eluting with *n*-hexane/ethyl acetate (50/1, v/v) to afford yellowish solid (105 mg, yield: 21%). ^1H NMR (400 MHz, CDCl_3): δ 9.48 (s, 1 H), 8.36 (d, $J = 2.0$ Hz, 1 H), 8.06 (dd, $J = 9.2$, 0.4 Hz, 1 H), 7.94 (dd, $J = 9.2$, 2.0 Hz, 1 H), 2.84 (s, 3 H).

Compound **6**. NBS (66 mg, 0.373 mmol) was added to a solution of 2-aminobenzaldehyde (45 mg, 0.373 mmol) in DMF (8 mL). The reaction mixture was stirred at r.t. for 1 h under N_2 atmosphere. The yellowish solution was poured into water and extracted with CH_2Cl_2 . Then the organic layer was washed with water four times, and the solvent was removed under reduced pressure. 67 mg yellow oil was obtained as the crude product, which was used immediately for the next step reaction without purification.

Saturated ethanolic KOH (10 mL) was added to a mixture of compound **5** (70 mg, 0.30 mmol) and 2-amino-5-bromobenzaldehyde (67 mg, 0.373 mmol in theory) in ethanol (40 mL), and the mixture was refluxed for 16 h under nitrogen atmosphere. After the mixture was cooled to r.t., water was added. The formed grey precipitate was collected by filtration and purified by column chromatography (silica gel, *n*-hexane/ethyl acetate = 500/7, v/v) to obtain white powder (84 mg,

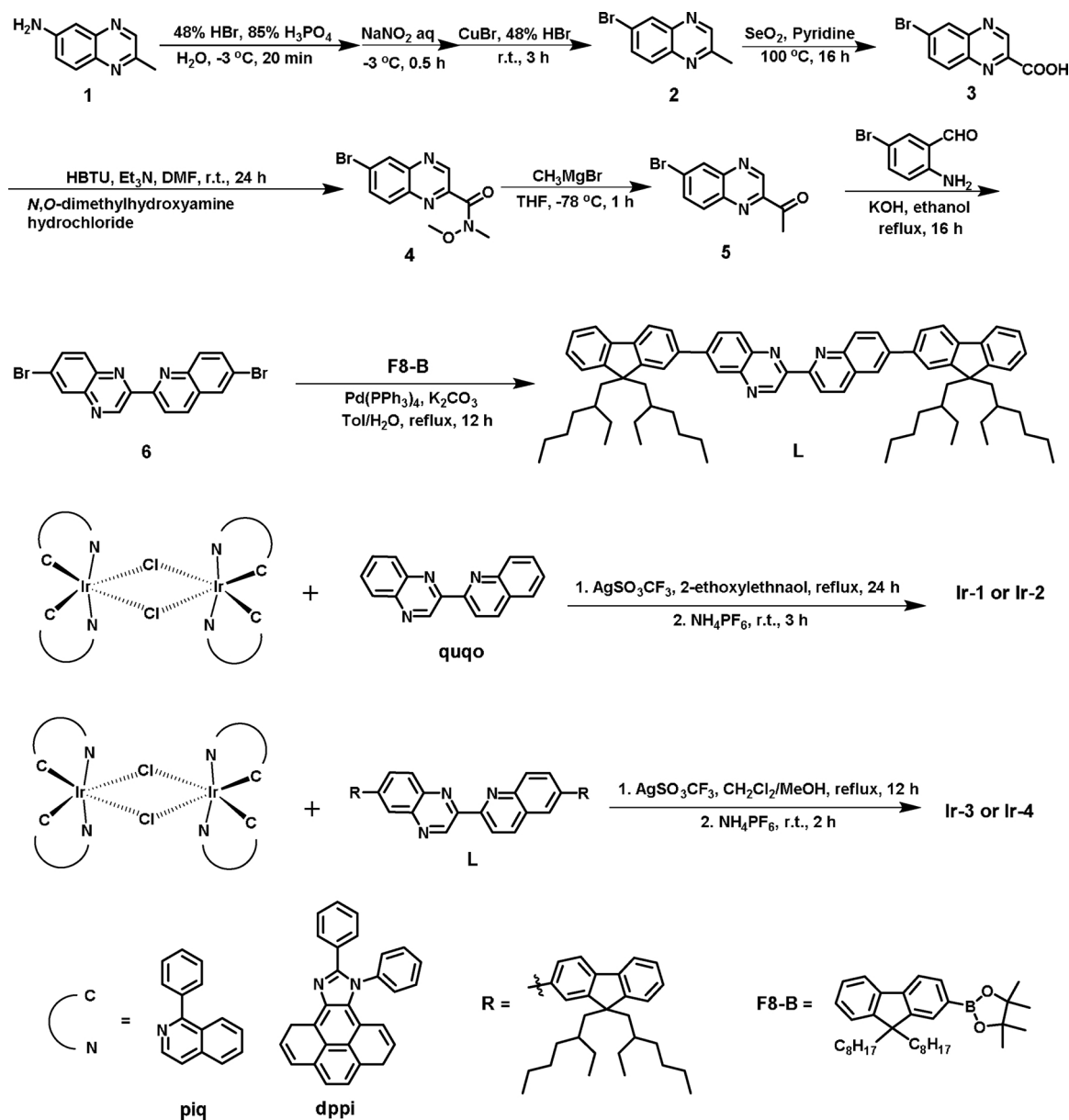
yield: 46%). ^1H NMR (400 MHz, CDCl_3): δ 10.19 (s, 1 H), 8.74 (d, $J = 8.4$ Hz, 1 H), 8.37 (d, $J = 2.4$ Hz, 1 H), 8.26 (d, $J = 8.8$ Hz, 1 H), 8.13 (d, $J = 9.2$ Hz, 1 H), 8.07 (d, $J = 2.4$ Hz, 1 H), 8.06 (d, $J = 4.0$ Hz, 1 H), 7.90 (dd, $J = 9.2$, 2.4 Hz, 1 H), 7.86 (dd, $J = 9.2$, 2.4 Hz, 1 H).

Ligand **L**. Compound **6** (96 mg, 0.231 mmol), **F8-B** (263 mg, 0.509 mmol) and $\text{Pd}(\text{PPh}_3)_4$ (54 mg, 0.046 mmol) were added to 20 mL of toluene. Then 6 mL of 2 M K_2CO_3 aq. solution (2.2 g in 8 mL H_2O) was added. The mixture was heated to reflux under nitrogen for 12 h. After that the mixture was poured into 50 mL of water and extracted with ethyl acetate. The combined organic layer was dried over anhydrous Na_2SO_4 . After the solvent was removed under reduced pressure, the residue was purified by column chromatography (silica gel, *n*-hexane/ethyl acetate = 50/1, v/v) to give yellow oil (110 mg, yield: 46%) as the product. ^1H NMR (400 MHz, CDCl_3): δ 10.26 (s, 1 H), 8.79 (d, $J = 8.4$ Hz, 1 H), 8.44 (t, $J = 2.4$ Hz, 1 H), 8.41 (d, $J = 8.0$ Hz, 1 H), 8.34 (d, $J = 9.2$ Hz, 1 H), 8.27 (d, $J = 8.8$ Hz, 1 H), 8.14 (dd, $J = 10.8$, 2.4 Hz, 1 H), 8.11 – 8.08 (m, 2 H), 7.83 – 7.70 (m, 7 H), 7.53 (dd, $J = 16$, 8.4 Hz, 1 H), 7.41 – 7.26 (m, 6 H), 2.07 – 2.03 (m, 8 H), 0.91 – 0.46 (m, 60 H). ESI-HRMS (m/z): calcd. for $[\text{C}_{75}\text{H}_{91}\text{N}_3 + \text{Na}]^+$, 1056.7111; found, 1056.7134. Anal. Calcd. for $\text{C}_{75}\text{H}_{91}\text{N}_3$ (%): C, 87.07; H, 8.87; N, 4.06. Found: C, 86.74; H, 8.83; N, 3.91.

2.1.2. Synthetic procedure for Ir(III) complexes Ir-1 and Ir-2

A mixture of chloro-bridged Ir(III) dimer (0.05 mmol), **quqo** (25.7 mg, 0.10 mmol), AgSO_3CF_3 (25.7 mg, 0.10 mmol), and 2-ethoxyethanol (10 mL) was heated to reflux under N_2 for 24 h. After the mixture was cooled to r.t., NH_4PF_6 (163 mg, 1 mmol) was added and stirred for another 3 h at r.t. Then water (50 mL) was added to get a green precipitate. The precipitate was collected by filtration, and washed with water and hexane, respectively. The crude product was purified by column chromatography (silica gel, *n*-hexane/ethyl acetate = 1:1, v/v) followed by recrystallization from CH_2Cl_2 and *n*-hexane.

Ir-1. Dark green powder 91 mg (yield: 86%). ^1H NMR (400 MHz, CDCl_3): δ 10.01 (s, 1 H), 8.86 – 8.71 (m, 3 H), 8.68 (d, $J = 8.8$ Hz, 1 H), 8.25 (d, $J = 8.0$ Hz, 1 H), 8.18 (d, $J = 8.4$ Hz, 1 H), 8.09 (dd, $J = 8.4$, 1.2 Hz, 1 H), 7.87 – 7.80 (m, 3 H), 7.78 (d, $J = 9.1$ Hz, 1 H), 7.75 – 7.61 (m, 7 H), 7.58 (d, $J = 6.4$ Hz, 1 H), 7.47 (ddd, $J = 8.0$, 6.8, 0.8 Hz, 1 H), 7.29 (dd, $J = 6.4$, 3.6 Hz, 2 H), 7.20 (ddd, $J = 8.8$, 7.2, 1.6 Hz, 1 H), 7.16 – 7.07 (m, 3 H), 6.92 – 6.85 (m, 2 H), 6.39 (dd, $J = 7.6$, 1.2 Hz, 1 H), 6.35 (dd, $J = 7.6$, 1.2 Hz, 1 H). ESI-HRMS (m/z) Calcd for $[\text{C}_{47}\text{H}_{31}\text{IrN}_5]^+$, 858.2206; found, 858.2236. Anal. Calcd. for

Scheme 1. Synthetic schemes for ligand **L** and the Ir(III) complexes **Ir-1** – **Ir-4**.

C₄₇H₃₁IrN₅PF₆·3H₂O (%): C, 53.41; H, 3.53; N, 6.63. Found: C, 53.59; H, 3.36; N, 6.72.

Ir-2. Dark green powder 82 mg (yield: 58%). ¹H NMR (400 MHz, CDCl₃): δ 8.95 (s, 1 H), 8.36 (d, *J* = 8.4 Hz, 1 H), 8.21 (dd, *J* = 8.0, 1.2 Hz, 1 H), 8.14 – 8.01 (m, 5 H), 8.00 – 7.80 (m, 11 H), 7.78 – 7.55 (m, 9 H), 7.51 (d, *J* = 8.4 Hz, 1 H), 7.43 – 7.28 (m, 3 H), 7.13 (t, *J* = 7.2 Hz, 2 H), 6.94 – 6.68 (m, 5 H), 6.63 – 6.57 (m, 2 H), 6.46 (dd, *J* = 8.0, 1.2 Hz, 1 H), 6.35 (t, *J* = 8.0 Hz, 1 H), 6.27 (t, *J* = 8.0 Hz, 1 H), 6.02 (dd, *J* = 8.0, 1.2 Hz, 1 H). ESI-HRMS (*m/z*): calcd. for [C₇₅H₄₅IrN₇]⁺, 1236.3367; found, 1236.3355. Anal. Calcd. for C₇₅H₄₅IrN₇PF₆·1.5H₂O (%): C, 63.96; H, 3.44; N, 6.96. Found: C, 63.91; H, 3.80; N, 6.89.

2.1.3. Synthetic procedure for Ir(III) complexes **Ir-3** and **Ir-4**

The solution of Ir(III) chloro-bridged dimer (0.02 mmol), ligand **L** (42 mg, 0.04 mmol) and AgSO₃CF₃ (10 mg, 0.04 mmol) in CH₂Cl₂/MeOH (45 mL, 2:1, v/v) was refluxed under nitrogen atmosphere for 12 h. After that, the dark red solution was cooled to room temperature, and a 10-fold excess of NH₄PF₆ (33 mg, 0.20 mmol) was added and stirred for 2 h at r.t. The volatiles were completely removed under

reduced pressure, and the residue was purified by column chromatography on silica gel using CH₂Cl₂/ethyl acetate (50:1, v/v) as the eluent to obtain the product. The product was further purified by recrystallization from CH₂Cl₂ and *n*-hexane.

Ir-3. Dark red powder 52 mg (yield: 68%). ¹H NMR (400 MHz, CDCl₃): δ 10.12 (s, 1 H), 8.96 (d, *J* = 6.8 Hz, 1 H), 8.88 (d, *J* = 7.6 Hz, 1 H), 8.79 (t, *J* = 9.2 Hz, 2 H), 8.41 (d, *J* = 1.6 Hz, 1 H), 8.29 (d, *J* = 6.4 Hz, 1 H), 8.23 (d, *J* = 7.6 Hz, 1 H), 8.07 (s, 1 H), 7.90 – 7.82 (m, 3 H), 7.78 – 7.48 (m, 17 H), 7.40 – 7.29 (m, 9 H), 7.17 – 7.11 (m, 1 H), 7.00 – 6.91 (m, 2 H), 6.45 (d, *J* = 8.0 Hz, 1 H), 6.41 (d, *J* = 8.0 Hz, 1 H), 2.07 – 1.97 (m, 8 H), 0.90 – 0.45 (m, 60 H). ESI-HRMS (*m/z*): calcd. for [C₁₀₅H₁₁₁IrN₅]⁺, 1634.8481; found, 1634.8529. Anal. Calcd. for C₁₀₅H₁₁₁IrN₅PF₆·7H₂O (%): C, 66.15; H, 6.61; N, 3.67. Found: C, 66.17; H, 6.87; N, 3.72.

Ir-4. Dark red powder 62 mg (yield: 72%). ¹H NMR (400 MHz, CDCl₃): δ 9.06 (s, 1 H), 8.47 (s, 1 H), 8.45 – 8.38 (m, 1 H), 8.34 – 8.22 (m, 2 H), 8.16 – 8.03 (m, 6 H), 8.09 – 7.91 (m, 7 H), 7.87 – 7.53 (m, 22 H), 7.42 – 7.30 (m, 8 H), 7.24 – 7.16 (m, 2 H), 6.94 – 6.76 (m, 3 H), 6.70 – 6.41 (m, 3 H), 6.17 – 6.02 (m, 1 H), 2.12 – 1.96 (m, 8 H), 0.94 –

0.37 (m, 60 H). ESI-HRMS (m/z): calcd. for $[C_{133}H_{125}IrN_7]^+$, 2012.9642; found, 2012.9677. Anal. Calcd. for $C_{133}H_{125}IrN_7PF_6$ (%): C, 74.00; H, 5.84; N, 4.54. Found: C, 73.64; H, 6.06; N, 4.68.

2.2. Photophysical and nonlinear transmission measurements

The UV-vis absorption spectra were recorded on a Shimadzu UV-2501 spectrophotometer. The steady-state emission was measured on a HORIBA FluoroMax-4 fluorometer/phosphorometer. The relative actinometry method [66] was used to determine the emission quantum yields in degassed solutions, with a degassed acetonitrile solution of $[Ru(bpy)_3]Cl_2$ ($\Phi_{em} = 0.097$, $\lambda_{ex} = 436$ nm) [67] being used as the reference for the complexes and 1 N sulfuric acid solution of quinine bisulfate ($\Phi_{em} = 0.546$, $\lambda_{ex} = 347.5$ nm) [68] was used as the reference for ligand **L**. The nanosecond transient difference absorption (TA) spectra and lifetimes were measured on an Edinburgh LP920 laser flash photolysis spectrometer in degassed toluene solutions. Excitation was provided by the third-harmonic output (355 nm) of a Quantel Brilliant Q-switched Nd:YAG laser (pulse width ~ 4.1 ns, the repetition rate was set to 1 Hz). The reverse saturable absorption of complexes **Ir-1** – **Ir-4** was demonstrated in CH_2Cl_2 solutions by a nonlinear transmission experiment at 532 nm using the Quantel Brilliant laser (pulse width ~ 4.1 ns, the repetition rate was set to 10 Hz) as the light source. The linear transmission of the sample solutions was adjusted to 80% at 532 nm in a 2-mm-thick cuvette. A 40-cm plano-convex lens was used to focus the beam to the center of the 2-mm-thick sample cuvette. The radius of the beam waist at the focal point was approximately 96 μm . The experimental setup and other details were described previously [23,69,70].

2.3. Computational methodology

Ground- and excited-state geometries were obtained at the level of density functional theory (DFT). The UV-vis absorption spectra and emission energies were simulated using the linear-response time-dependent DFT (TDDFT). All calculations were carried out using Gaussian09 quantum chemistry software package [71]. The effect of toluene solvent was implicitly included using Conductor Polarized Continuum Model (CPCM) [72,73]. The ground-state geometry was optimized in toluene using PBE0 functional [74] with the mixed basis set applying LAN2DZ [75,76] for Ir(III) and 6-31G* [77–81] for C, H and N atoms.

Our previous studies showed that PBE0 functional was capable to accurately represent the UV-vis absorption spectra of heteroleptic monocationic Ir(III) complexes [29]. However, this functional resulted in an inconsistent trend of the lowest-energy absorption band for **Ir-3** and **Ir-4**, compared to their experimental spectra (Supporting Information (SI) Fig. S1). Many research results on DFT methods pointed out that for all practical applications every DFT model serves as an effective approximate method and is able to correctly describe only a specific realm of physical phenomena. Intent to only reproduce experimentally measured quantities frequently led to incorrect interpretations (i.e., getting the right number for the wrong reason) [82]. Taking this point into account, we compared the performance of PBE0 and ω B97XD in reproducing the absorption spectra of **Ir-1** – **Ir-4** (SI Fig. S1). While PBE0 provided much better agreement for the energies of absorption bands of all complexes, it resulted in a reverse trend for the low-energy charge transfer (CT) band between **Ir-3** and **Ir-4**. In contrast to the hybrid functionals like PBE0, which include a fixed portion of the Hartree Fock (HF, 25%) exchange to the pure generalized gradient approximation (GGA) exchange, the long range corrected (LRC) functionals have HF contributions depending on the inter-electronic distances. For instance, the functional ω B97XD has 22% HF exchange contributing in the short-range, whereas 100% HF contribution in the long range. The variable HF fractions of orbital exchange to some extent eliminate the spurious long-range self-repulsion intrinsic to GGA

functionals. This typically leads to more accurate descriptions of the CT character of excitonic states compared to the hybrid functionals such as PBE0. However, the energies of the optical transitions are highly sensitive to the HF portion: the higher the HF portion the larger the transition energy. Therefore, ω B97XD that includes up to 100% HF in long-range typically results in over-blue-shifted absorption bands compared to the experimental spectra [83,84].

It is also well-known that the HF portion in functionals affects the CT and π, π^* transitions differently. While both transitions are shifted to the blue with increased HF contributions to the functional, the CT states are shifted much more than the π, π^* states [82,85–88]. Because of the more pronounced CT character of the lowest-energy band in **Ir-3** than in **Ir-4**, ω B97XD functional resulted in more blue-shifted lowest-energy S_1 transition in **Ir-3** than that in **Ir-4**, while PBE0 provided a reverse trend (SI Fig. S1). Despite the significantly blue-shifted energies, the trend of the calculated absorption spectra of **Ir-1** – **Ir-4** by ω B97XD qualitatively agreed with the experimental spectra. Based on its reliable qualitative trend, ω B97XD functional was chosen for calculations of the absorption spectra despite the overestimated energies of optical transitions. Thus, 60 optical transitions were calculated by TDDFT using ω B97XD functional and the mixed LANL2DZ/6-31G* basis set in toluene to reproduce the absorption spectra of the ligand **L** and complexes **Ir-1** – **Ir-4**. Broadening the obtained transitions by a normalized Gaussian function with a line-width of 0.1 eV made the calculated UV-vis absorption spectral profiles qualitatively agree with the experimental spectra. The characteristics of each transition were analyzed by generating natural transition orbitals (NTOs) [89] and visualized via GaussView 5.09 graphical software [90] using an isovalue of 0.02 (SI Fig. S2).

The phosphorescence energies were simulated by analytical TDDFT [91] via optimizing the excited triplet state using PBE0 functional. Characterization of the nature of the emissive states via NTOs utilizing PBE0 gave rise to the consistent results with the experimental evidence. In contrast, simulating the emissive states via Δ SCF-TDDFT [92] utilizing ω B97XD resulted in all transitions having $^3\pi, \pi^*$ character (SI Table S1). The large percentage of HF and LRC in ω B97XD caused the CT transitions to shift above the $^3\pi, \pi^*$ optical transitions, which are inconsistent with the excited state lifetimes.

3. Results and discussion

3.1. Synthesis and characterization

As mentioned earlier, the purpose of incorporating fluorene units to the diimine ligand **L** is to improve the triplet lifetime of the formed Ir(III) complexes. However, the synthesis of **L** was quite challenging and suffered from harsh reaction conditions, precautionary experimental operation, careful purification and low reaction yield due to the instability of the 6-Br-substituted quinoxaline derivatives in the presence of acid, base or nucleophilic reagents. The synthetic schemes for ligand **L** and its precursors are outlined in Schemes 1 and S1. Preparation of the key precursor (compound **6**) started with 6-amino-2-methylquinoxaline (compound **1**) via diazotization-bromination, oxidation, Weinreb–Nahm ketone synthesis and Friedländer condensation (Scheme 1). In the first step reaction to obtain 6-bromo-2-methylquinoxaline (compound **2**), direct cyclization of 4-bromo-1,2-diaminobenzene and pyruvic aldehyde frequently yielded a mixture of 6- and 7-brominated 2-methylquinoxaline, which was very difficult to separate [93–95]. Instead, diazotization-bromination is the most commonly used method for preparing aryl bromides, and the major advantage of this approach is the selective bromination to a specific position on the aromatic ring [96,97]. After screening a variety of strong acids and optimizing reaction temperature [98–100], the diazotization-bromination reaction was carried out using sodium nitrite at $-3 \sim 5^\circ C$ in two steps: diazotization of the amine in concentrated hydrobromic and phosphoric acid mixture and a subsequent reaction with concentrated

hydrobromic acid in the presence of cuprous bromide. A small-scale reaction of 0.5 mmol starting compound was found to be the most appropriate stoichiometry for our experimental condition. Precise temperature and reaction time control, and the speed for acid addition also affected the yield of this reaction pronouncedly, which was lowered due to the loss of bromine or producing bi-brominated byproduct. The next two steps, *i.e.* oxidation and Weinreb–Nahm amination reactions proceeded with high yields, showing that the 6-bromo substituent was inert under such a reaction condition [101]. The subsequent treatment of Weinreb–Nahm amine (compound 4) with a Grignard reagent for ketone formation at -78°C only gave 21% isolated yield because the strong nucleophilic Grignard reagent replaced the 6-bromo group even at a very low reaction temperature. It should be noted that attempts to substitute 6-bromo with fluorenyl group by a Suzuki or Stille coupling reaction prior to the formation of ketone failed. The Friedländer condensation reaction to form the key intermediate 6 and the subsequent Suzuki coupling reaction to produce ligand L both showed low yields. Moreover, the side reaction that led to mono substituted byproduct formation caused the difficulty in purification of the Suzuki coupling reaction. All compounds except for compound 3 were purified by column chromatography.

The synthesis of **Ir-1** and **Ir-2** followed the classic reaction condition using the corresponding chloro-bridged Ir(III) dimer and the quqo ligand via the bridge-splitting reaction in the presence of AgSO_3CF_3 at high temperature. However, the synthesis of **Ir-3** and **Ir-4** followed a modified procedure that utilized AgSO_3CF_3 salt and a mixed low boiling point solvents CH_2Cl_2 and MeOH. This milder reaction condition avoided high-temperature reaction, reduced complicated side reactions and shortened the reaction time. Consequently, **Ir-3** and **Ir-4** showed a reduced decomposition at this reaction condition and the production yields were higher compared to the traditional preparation procedures [26]. Care should be taken when using MeOH as eluent in the process of column chromatography because complexes **Ir-3** and **Ir-4** were completely decomposed. All new compounds were identified by ^1H NMR spectroscopy, and the ligand L and Ir(III) complexes were further characterized by high resolution ESI-mass spectrometry and elemental analyses. It is worth noting that ligand L and the Ir(III) complexes showed good air-stability and solubility in common organic solvents.

3.2. Electronic absorption

The experimental and calculated UV–vis absorption spectra of the ligand L and Ir(III) complexes are shown in Fig. 1. The overall spectral features and absorption bands matched well between the experimental and theoretical spectra except for the ca. 40–80 nm blue-shifts of absorption bands in the theoretical spectra (SI Fig. S2). The electronic absorption band maxima and molar extinction coefficients data are listed in Table 1. Although planar π -conjugated ligands existed in the cyclometalating and diimine ligands, no ground-state aggregation was observed in the concentration range studied for the Ir(III) complexes in toluene ($1 \times 10^{-6} - 1 \times 10^{-4} \text{ mol L}^{-1}$). The absence of aggregation should be mainly ascribed to the octahedral geometry of the Ir(III) complexes, which prevents intermolecular interactions and is a common feature for Ir(III) complexes [102,103].

As shown in Fig. 1, the diimine ligand L displayed two major absorption bands at 292 and 388 nm, respectively, with large molar extinction coefficients (over $10^4 \text{ L mol}^{-1} \text{ cm}^{-1}$, Table 1). According to the reports on the related diimine ligands, these bands should predominantly originate from the $^1\pi, \pi^*$ transitions, possibly mixed with some $^1\text{ILCT}$ configuration in the 388-nm band [34,57].

All Ir(III) complexes displayed intense absorption bands in the spectral regions of $< 400 \text{ nm}$ (420 nm in **Ir-4**), moderately intense absorption bands in the range of 400–520 nm (420–570 nm in **Ir-4**), and weak absorption bands at $> 520 \text{ nm}$ ($> 570 \text{ nm}$ in **Ir-4**). Considering the vibronic structures of the high-energy absorption bands at < 400 or 420 nm and their large molar extinction coefficients ($\epsilon > 10^4$

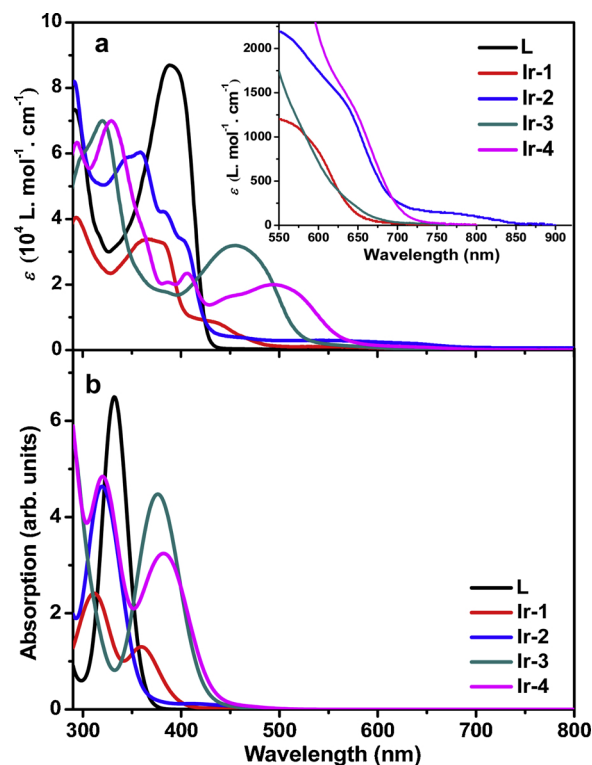


Fig. 1. UV–vis absorption spectra of ligand L and Ir(III) complexes **Ir-1**–**Ir-4** in toluene. (a) Experimental spectra. The inset shows the expanded spectra in the regions of 550 – 900 nm. (b) TDDFT calculated spectra in toluene using ωB97XD functional.

$\text{L mol}^{-1} \text{ cm}^{-1}$, Table 1), these bands are assigned to the spin-allowed intraligand (^1IL) $^1\pi, \pi^*$ transitions [34,49–52,57], maybe mixed with minor charge-transfer characters with reference to our previously reported quqo based Ir(III) complexes [34]. While the moderately intense absorption bands at 400–520 nm (or 420–570 nm in **Ir-4**) are broad and structureless, which typically arise from charge transfer transitions such as ligand-to-ligand charge transfer ($^1\text{LLCT}$) and/or metal-to-ligand charge transfer ($^1\text{MLCT}$) with reference to the other reported Ir(III) complexes [104,105]. For complexes **Ir-3** and **Ir-4**, the absorption bands in this spectral region are much stronger. In view of the structural feature of the diimine ligand in these two complexes that contains electron-donating fluorenyl substituents and electron-withdrawing quqo component, these bands likely predominantly originate from intraligand charge transfer ($^1\text{ILCT}$) transitions within the diimine ligand mixed with some $^1\text{LLCT}/^1\text{MLCT}$ characters. The very weak and broad tails at 500–700 nm for **Ir-1**, 500–850 nm for **Ir-2**, 550–700 nm for **Ir-3**, and 570–750 nm for **Ir-4** could be an overlay of multiple sources of transitions. Based on the previous reports on other Ir(III) complexes, $^3\text{MLCT}$, $^3\pi, \pi^*$, and $^3\text{LLCT}$ transitions could contribute to the bands in this region [29,34,36]. The energy of this band in **Ir-1** was quite similar to those reported for other Ir(III) complexes bearing the same quqo ligand [34]. In contrast, this band in **Ir-2** became much stronger compared to that in **Ir-1** and extended to 850 nm. This phenomenon could be attributed to the extended π -conjugation of the dpqi ligands, which raised the dpqi-localized highest occupied molecular orbital (HOMO) and reduced the energies of the $^1,^3\text{LLCT}$ transitions. However, incorporation of the electron-donating fluorenyl motif to the quqo ligand in **Ir-4** shortened this band to 750 nm (see Fig. 1a inset). This change can be presumably ascribed to the destabilized quqo-localized lowest unoccupied molecular orbital (LUMO) due to the extended π -conjugation of the diimine ligand and the electron-donating ability of the fluorene motif, which in turn increased the energies of the $^1,^3\text{LLCT}$ transitions.

Table 1
Photophysical parameters of the ligand **L** and Ir(III) complexes **Ir-1** – **Ir-4**.

	$\lambda_{\text{abs}}/\text{nm}$ ($\log \epsilon$) ^a	$\lambda_{\text{em}}/\text{nm}$ ($\tau_{\text{em}}/\text{ns}$); Φ_{em} ^b	$\lambda_{\text{T1-Tn}}/\text{nm}$ ($\tau_{\text{T}}/\text{ns}$) ^c
L	388 (4.94), 292 (4.87)	430 (–), 453 (–); 0.32	490 (60,000), 690 (60,000)
Ir-1	550 (3.08), 432 (3.94), 381 (4.52), 366 (4.53), 293 (4.61)	612 (–), 659 (–); –	407 (–)
Ir-2	750 (2.20), 621 (3.19), 548 (3.45), 464 (3.59), 402 (4.53), 382 (4.63), 358 (4.78), 345 (4.77), 290 (4.91)	704 (–); –	436 (–)
Ir-3	568 (3.11), 455 (4.51), 384 (4.25), 320 (4.85), 299 (4.78)	703 (60); 0.0037	525 (60)
Ir-4	625 (3.21), 495 (4.30), 448 (4.22), 406 (4.37), 387 (4.32), 329 (4.84), 294 (4.80)	706 (50); 0.0034	570 (50)

^a Absorption band maxima and molar extinction coefficients of the UV–vis absorption in toluene at r.t.

^b Emission band maxima and decay lifetimes in degassed toluene at r.t. (1×10^{-5} mol/L). A degassed acetonitrile solution of [Ru(bpy)₃]Cl₂ ($\Phi_{\text{em}} = 0.097$, $\lambda_{\text{ex}} = 436$ nm) [67] was used as the reference for the complexes and 1 N sulfuric acid solution of quinine bisulfate ($\Phi_{\text{em}} = 0.546$, $\lambda_{\text{ex}} = 347.5$ nm) [68] was used as the reference for ligand **L** emission quantum yield measurements at r.t.

^c Nanosecond TA band maxima and triplet excited-state lifetimes in degassed toluene at r.t.

In order to unambiguously assign the nature of the absorption bands, TDDFT calculations were carried out and the natural transition orbitals (NTOs) of the major transitions contributing to the low-energy absorption bands for the ligand **L** and Ir(III) complexes are compiled in Table 2. The NTOs of the other major transitions contributing to the bands below 400 nm are provided in Table S2 of the Supporting Information. As depicted in Table 2, the holes of the low-energy transitions in the complexes are delocalized on the phenyl motifs of the C[∞]N ligand, the *d*-orbital of the Ir(III) ion, the pyrenylimidazole components of the dppl ligand in case of **Ir-2** and **Ir-4**, and part of the diimine ligand in **Ir-3** and **Ir-4** (see holes of S₂ and S₄ states for **Ir-3** and S₃ state for **Ir-4** in Table 2), while the electrons are exclusively localized on the **quqo** ligand. Therefore, the absorption bands between 400 and 520 nm (or 420–570 nm in **Ir-4**) indeed corresponded to the ¹LLCT/¹MLCT (for **Ir-1** and **Ir-2**) and ¹ILCT/¹LLCT/¹MLCT (for **Ir-3** and **Ir-4**) transitions in nature, which agreed with our aforementioned assignments based on the features of the absorption bands. For the high energy absorption bands at < 400 nm, NTOs (see NTOs in Table S2) indicate that both the holes and electrons are essentially localized on the same C[∞]N or diimine ligands, which supports the ligand-centered ¹ π, π^* transitions mixed with minor ¹LLCT/¹MLCT transitions.

3.3. Photoluminescence

Emission characteristics of the ligand **L** and complexes **Ir-1–Ir-4** were investigated in different solvents at room temperature. The emission spectra in toluene are displayed in Fig. 2, and the emission band maxima, lifetimes and quantum yields are listed in Table 1. The emission spectra and parameters in other solvents are provided in the Supporting Information Fig. S5 and Table S3.

The ligand **L** exhibited structured blue fluorescence with a moderate quantum yield in toluene ($\Phi_{\text{em}} = 0.32$) and hexane ($\Phi_{\text{em}} = 0.26$). However, the emission spectra became featureless and gradually red-shifted when the polarity of solvent increased from dichloromethane, acetone to acetonitrile, accompanied by much higher fluorescence quantum yields of 0.60–0.68 compared to those in toluene and hexane. In addition, the fluorescence quantum yields slightly decreased in more polar solvents acetone and acetonitrile compared to that in dichloromethane. These features imply that the observed blue fluorescence in the nonpolar solvents toluene and hexane emanates from a ¹ π, π^* state; while the emitting state changes to an intramolecular charge transfer state (¹ICT) in polar solvents.

In contrast, complexes **Ir-1–Ir-4** are all very weakly emissive at room temperature in solutions. The emission quantum yields of **Ir-1** and **Ir-2** were too low to be reliably determined. All complexes exhibited far-red to NIR phosphorescence with emission maxima at 659 nm for **Ir-1** to approximately 706 nm for **Ir-2–Ir-4**. The assignment of the emission to phosphorescence is based on the facts of significant red-shifts of the emission bands with respect to the corresponding excitation wavelengths (i.e. > 5000 cm^{−1}), prone to oxygen quenching (SI Fig. S6), and the tens of nanosecond emission lifetimes for **Ir-3** and **Ir-4** (Tables 1 and

S3, and Fig. S7). In view of the relatively short phosphorescence lifetimes and the broad spectral feature, the nature of the emitting states could have predominant charge transfer (³CT) character, likely being the ³MLCT/³LLCT states but with significant ³ILCT configurations in case of **Ir-3** and **Ir-4**. However, the spectra of **Ir-1** and **Ir-4** are somewhat structured, implying some involvement of the ligand-localized ³ π, π^* configuration.

The involvement of ³ π, π^* configuration in the emitting state of **Ir-1** is partially supported by its similar emission feature to that of (piq)₂Ir(bpy)²⁺ (bpy = bipyridine), which also showed structured emission at 592 and 630 nm in toluene with the mixed ³MLCT/³LLCT/³ π, π^* (piq-localized) parentage [24]. The red-shifted emission spectrum of **Ir-1** compared to that of (piq)₂Ir(bpy)²⁺ reflects the nature of the strong electron-withdrawing ability and extended π -conjugation of the **quqo** ligand, which decreased the energy of the ³MLCT/³LLCT state and significantly increased the nonradiative decay rate. Consequently, the emission of **Ir-1** was too weak to allow for the emission quantum yield and lifetime to be reliably determined. For **Ir-2**, the predominant charge transfer nature of its emitting state was supported by its drastically red-shifted emission spectrum (704 nm in toluene) and very weak emission in comparison to its (dppl)₂Ir(bpy)²⁺ counterpart (568 nm, with a lifetime of 12.2 μ s and quantum yield of 0.0064 in toluene) that has a dppl-localized ³ π, π^* emitting state [24]. In addition, the expansive π -conjugation of the **dppl** ligand increased the HOMO energy level (SI Fig. S3) and reduced the energy of the emitting ³MLCT/³LLCT state of complex **Ir-2**, leading to the further red-shifted emission with respect to **Ir-1**.

For complexes **Ir-3** and **Ir-4**, the involvement of ³ILCT configuration in their emitting states is partially supported by the positive solvatochromic effect (SI Fig. S5). In addition, the similar emission energies, quantum yields and lifetimes of these two complexes imply that the emission of these two complexes mainly come from the same structural component, i.e. the fluorenyl-substituted **quqo** ligand, which is associated with the ³ π, π^* /³ILCT state. However, the emission spectrum of **Ir-4** showed a clearer vibronic structure, suggesting more ³ π, π^* character in the emitting state of **Ir-4**.

To better understand the nature of the emitting states in **Ir-1–Ir-4**, analytical TDDFT calculations were carried out using PBE0 functional. The NTOs contributing to the lowest triplet excited state are shown in Table 3. Although the calculated energies were noticeably red-shifted compared to the experimental data, the trend of the calculated energies of the lowest triplet transitions essentially matched the emission energy trend of the experimental spectra ($\Delta E_{\text{Ir-1}} > \Delta E_{\text{Ir-2}} \approx \Delta E_{\text{Ir-3}} \approx \Delta E_{\text{Ir-4}}$), allowing one to make meaningful reference. As the NTOs of **Ir-1** and **Ir-2** indicate, the holes are mainly on the cyclometalating C[∞]N ligand, the *d* orbitals of the Ir(III) metal ion, and a very small portion of the **quqo** ligand in case of **Ir-1**; while the electrons are exclusively on the **quqo** ligand. Therefore, the emitting triplet excited states (T₁) should be the ³MLCT/³LLCT states for these two complexes mixed with minor ³ π, π^* character in case of **Ir-1**. In contrast, for **Ir-3** and **Ir-4**, both the holes and electrons primarily localized on the diimine ligand **L**, with some

contributions from the *d* orbital of the Ir(III) ion on the electrons. This distribution indicates that the observed emission of these two complexes emanates from the $^3\text{ILCT}/^3\pi,\pi^*/^3\text{MLCT}$ states, but **Ir-4** has more $^3\pi,\pi^*$ character. In **Ir-4**, the electrons also distributed to the **dppi** ligand. Thus, $^3\text{LLCT}$ configuration also contributed to its emitting state. These assignments essentially coincided with our assignments based on the experimental results.

3.4. Transient absorption (TA)

Nanosecond transient absorption measurements were employed to gain further insight into the absorption and lifetimes of the triplet excited states of ligand **L** and complexes **Ir-1** – **Ir-4**. Especially for the

Table 2

Natural transition orbitals (NTOs) representing transitions contributing to the low-energy bands of ligand **L** and Ir(III) complexes **Ir-1** – **Ir-4** in toluene.^a

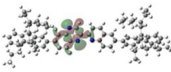
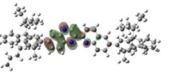
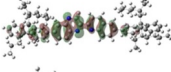
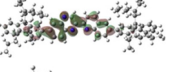
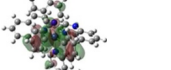
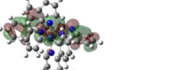
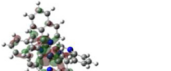
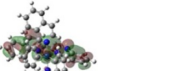
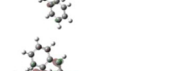
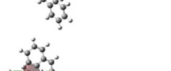
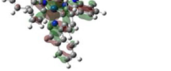
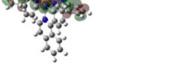
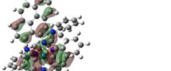
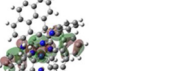
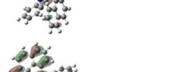
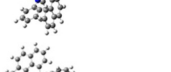
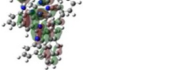

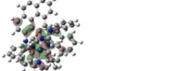
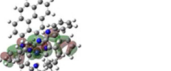
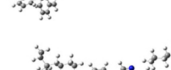
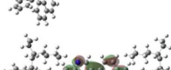
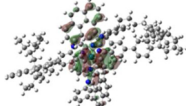
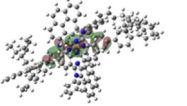
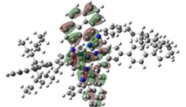
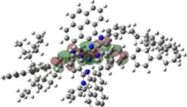
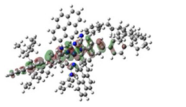
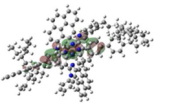
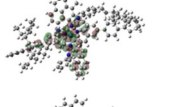
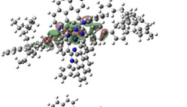
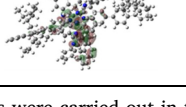
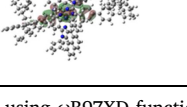
	Excited states and properties	Holes	Electrons
L	S_1 334 nm $f = 0.380$		
	S_2 332 nm $f = 1.925$		
Ir-1	S_1 439 nm $f = 0.080$		
	S_2 385 nm $f = 0.013$		
	S_3 376 nm $f = 0.068$		
Ir-2	S_1 456 nm $f = 0.019$		
	S_2 413 nm $f = 0.036$		
	S_3 377 nm $f = 0.018$		
Ir-3	S_1 436 nm $f = 0.022$		
	S_2 388 nm $f = 0.895$		
	S_4 370 nm $f = 0.664$		

Table 2 (continued)

	Excited states and properties	Holes	Electrons
Ir-4	S_1 458 nm $f = 0.023$		
	S_2 415 nm $f = 0.045$		
	S_3 393 nm $f = 0.777$		
	S_5 371 nm $f = 0.427$		
	S_6 364 nm $f = 0.309$		

^a TDDFT calculations were carried out in toluene using ωB97XD functional with mixed basis set of LANL2DZ/6-31G*, the geometries were obtained by ground state optimization using PBE0 with mixed basis set of LANL2DZ/6-31G*. The solvent effects for toluene were implicitly included using CPCM reaction field model.

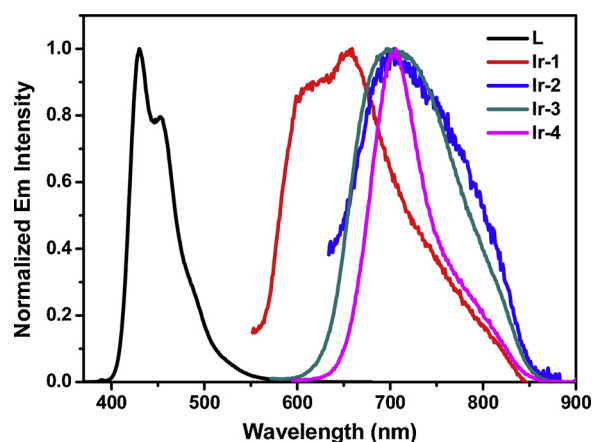
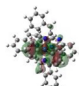
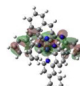
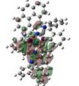
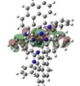
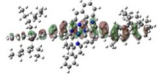
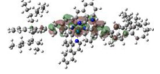
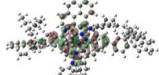
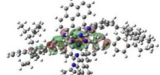


Fig. 2. Normalized emission spectra of ligand **L** and Ir(III) complexes **Ir-1** – **Ir-4** in toluene at r.t. (1×10^{-5} mol L⁻¹, $\lambda_{\text{ex}} = 347.5$ nm for **L**, 431 nm for **Ir-1**, 455 nm for **Ir-2** and **Ir-3**, and 495 nm for **Ir-4**). The toluene solutions of **Ir-1** – **Ir-4** were degassed by bubbling with N₂ for 40 min..

weaker or non-emissive species, such as complexes **Ir-1** and **Ir-2**, transient absorption spectroscopy is a better method to study the dynamics of the excited species. The TA spectra of complexes **Ir-1** – **Ir-4** at zero delay after excitation and the time-resolved TA spectra of complexes **Ir-3** and **Ir-4** upon excitation at 355 nm in deaerated toluene solutions are shown in Fig. 3. The time-resolved TA spectra of ligand **L** and complexes **Ir-1** and **Ir-2** are provided in Fig. S8 of the Supporting Information. The triplet excited-state lifetimes deduced from the decays of the TA signals (SI Fig. S9) are presented in Table 1. Because of the very weak TA signals from **Ir-1** and **Ir-2**, their triplet lifetimes were unable to be determined.

As shown in Fig. 3, both **Ir-1** and **Ir-2** exhibited very weak excited-state absorption in the regions of 400–600 nm. With reference to the

Table 3
NTOs contributing to the lowest triplet excited states of **Ir-1**–**Ir-4** in toluene.

	T ₁ energy (nm)	Electrons	Holes
Ir-1	836		
Ir-2	870		
Ir-3	911		
Ir-4	869		

nature of the emitting excited states discussed in the photoluminescence section, it is reasonable to attribute the observed TA to the $^3\text{MLCT}/^3\text{LLCT}$ states in these two complexes. Compared to the previously reported complexes $(\text{piq})_2\text{Ir}(\text{bpy})^{2+}$ and $(\text{dppi})_2\text{Ir}(\text{bpy})^{2+}$ (which have the same C'N ligand as that in **Ir-1** and **Ir-2**, respectively, but different diimine ligand) with broad and intense TA and μs -long triplet excited state lifetimes [24], the spectral features, intensities, and lifetimes of **Ir-1** and **Ir-2** are drastically different. This provides another piece of evidence that the natures of the T₁ states in **Ir-1** and **Ir-2** are indeed different from the $^3\pi,\pi^*$ states in the reported complexes. Again, this change is consistent with the lower-energy of the $^3\text{MLCT}/^3\text{LLCT}$ states in **Ir-1** and **Ir-2** due to the extended π -conjugation of the **quqo** ligand and its stronger electron-withdrawing ability, which make the $^3\text{MLCT}/^3\text{LLCT}$ states lower in energy than the C'N ligand-localized $^3\pi,\pi^*$ states and become the lowest triplet excited states.

Distinct from the TA spectra of **Ir-1** and **Ir-2**, the spectra of **Ir-3** and

Ir-4 resembled each other with a bleaching band occurring at 455 nm for **Ir-3** and 470 nm for **Ir-4**, and a broad positive absorption band at 495–800 nm for **Ir-3** and 515–800 nm for **Ir-4**. Both the bleaching and TA band maximum of **Ir-4** are obviously red-shifted compared to those in **Ir-3**, implying the impact of the different C'N ligands in these two complexes. The energies of the bleaching bands are in line with those of the $^1\pi,\pi^*/^1\text{ILCT}/^1\text{MLCT}/^1\text{LLCT}$ transitions in their respective ground-state absorption bands. The triplet lifetimes deduced from the decay of the TA signals (SI Fig. S9) are essentially the same as those obtained from the decay of emission, indicative of the origin of the observed TA being arising from the emitting T₁ states. With reference to the natures of the T₁ states discussed in the photoluminescence section, the observed TA for **Ir-3** and **Ir-4** are attributed to the $^3\text{MLCT}/^3\text{ILCT}/^3\pi,\pi^*$ states, mixed with some $^3\text{LLCT}$ character in case of **Ir-4**. Obviously, involvement of the diimine ligand-localized $^3\text{ILCT}/^3\pi,\pi^*$ configuration in the T₁ states dramatically enhanced the triplet excited-state absorption and prolonged the T₁ lifetimes in **Ir-3** and **Ir-4**. It should be noted that even if the transient absorbing species in **Ir-3** and **Ir-4** are quite similar, the TA signals of **Ir-4** are much weaker than those of **Ir-3**. This can be rationalized by the nature of TA measurement, which measures the absorption difference between the excited state and the ground state. Because of the distinct ground-state absorption spectral features of **Ir-3** and **Ir-4** (in view of the absorption band maxima and molar extinction coefficients, see Fig. 1), the observed TA intensities for these two complexes are different even if the excited-state absorption spectral features are similar.

3.5. Reverse saturable absorption (RSA)

Nonlinear transmission experiment was carried out to demonstrate the RSA of **Ir-1** – **Ir-4** in CH_2Cl_2 at 532 nm for ns laser pulses. CH_2Cl_2 was chosen as the solvent instead of toluene because it can dissolve the complexes better to reach the desired concentration. Fig. 4 displays the results for solutions with a linear transmittance of 80% in a 2 mm cuvette. All complexes exhibited a decrease of light transmission with increasing incident fluence, illustrating the appearance of RSA from

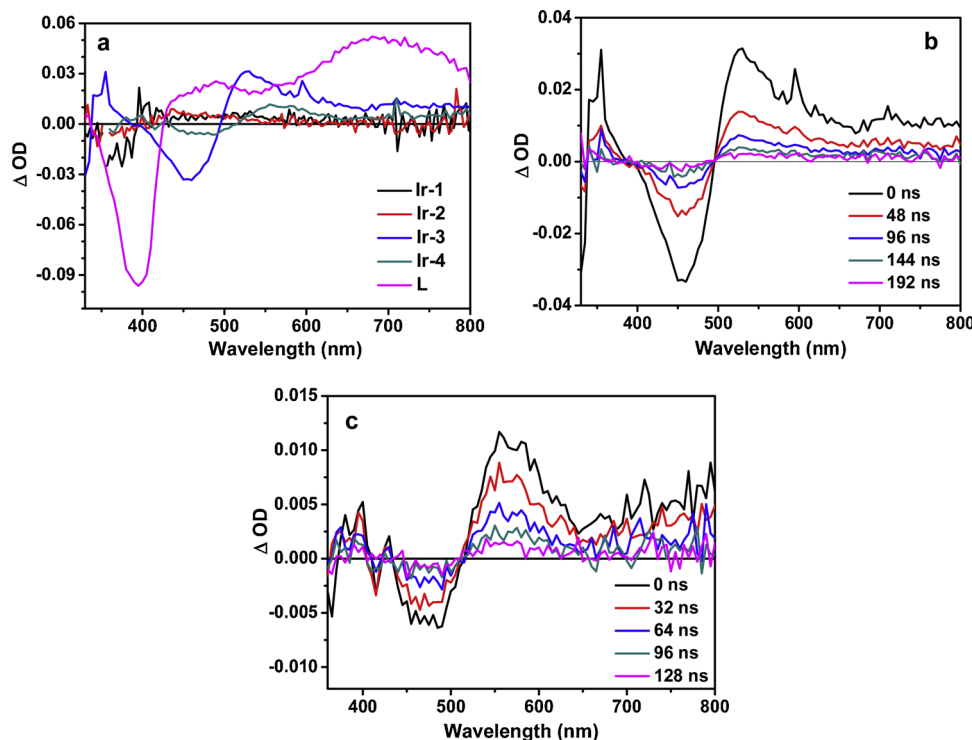


Fig. 3. (a) Nanosecond transient absorption spectra of ligand **L** and complexes **Ir-1** – **Ir-4** in degassed toluene at zero-time delay after excitation. (b) and (c) Nanosecond time-resolved transient absorption spectra of complexes **Ir-3** and **Ir-4** in degassed toluene, respectively. $\lambda_{\text{ex}} = 355 \text{ nm}$, $A_{355 \text{ nm}} = 0.4$ in a 1-cm cuvette.

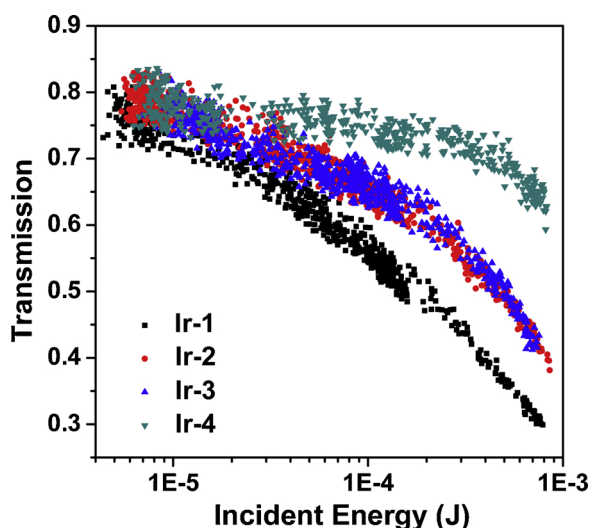


Fig. 4. Nonlinear transmission plots of complexes **Ir-1** – **Ir-4** at the linear transmittance of 80% in CH_2Cl_2 solutions in a 2-mm cuvette for 532-nm 4.1-ns laser pulses. The radius of the beam waist at the focal point was approximately 96 μm .

these complexes. When the incident fluence increased to 2.7 J/cm^2 , the transmission decreased to 0.29, 0.37, 0.40, and 0.58 for complexes **Ir-1**, **Ir-2**, **Ir-3** and **Ir-4**, respectively. The RSA strength of these complexes followed the trend of **Ir-1** > **Ir-2** \approx **Ir-3** > **Ir-4**. The occurrence of RSA at 532 nm for these complexes is consistent with their positive TA signals at 532 nm, which implies a stronger excited-state absorption relative to the ground-state absorption, even though the ΔOD values for complexes **Ir-1** and **Ir-2** are very small at this wavelength.

It is known that the ratio of the excited-state absorption cross section (σ_{ex}) vs. the ground-state absorption cross section (σ_0) is the critical parameter that determines the strength of RSA. Unfortunately, the σ_{ex} values could not be deduced using the commonly used singlet depletion method because of the influence of stronger ground-state absorption at 532 nm ($\epsilon > 10^3 \text{ L mol}^{-1} \text{ cm}^{-1}$) in these complexes. Nonetheless, we still can roughly correlate the observed RSA performance to their ground-state absorption cross sections obtained from the UV–vis absorption spectra and the ΔOD values obtained from the TA spectra at 532 nm. The much stronger RSA of **Ir-1** compared to that of **Ir-2** should be mainly attributed to its much weaker ground-state absorption at 532 nm (Fig. 1) because the ΔOD values for these two complexes at 532 nm are quite similar. Weaker ground-state absorption increased the $\sigma_{\text{ex}}/\sigma_0$ ratio and thus enhanced the RSA of **Ir-1**. This trend resembled the trend that we found in Ir(III) complexes $(\text{piq})_2\text{Ir}(\text{bpy})^+$ (transmission decreased to 0.21) and $(\text{dppi})_2\text{Ir}(\text{bpy})^+$ (transmission decreased to 0.30) [24], which contained the same set of C^N ligands as those in **Ir-1** and **Ir-2**, respectively, but a different diimine ligand bpy. However, comparing the transmittance of **Ir-1** to $(\text{piq})_2\text{Ir}(\text{bpy})^+$ and **Ir-2** to $(\text{dppi})_2\text{Ir}(\text{bpy})^+$ at the same incident fluence, the RSA of **Ir-1** and **Ir-2** is weaker than their corresponding counterpart $(\text{piq})_2\text{Ir}(\text{bpy})^+$ and $(\text{dppi})_2\text{Ir}(\text{bpy})^+$, respectively. This indicates that the RSA of the Ir(III) complexes based on **quqo** diimine ligand is lower than that of the **bpy**-based Ir(III) complexes because benzannulation and incorporation of the additional N atom on the diimine ligand red-shifted the charge-transfer absorption bands in **Ir-1** and **Ir-2** and thus increased the ground-state absorption at 532 nm.

For **Ir-3** and **Ir-4**, although their ΔOD values at 532 nm are much larger compared to those in **Ir-1** and **Ir-2**, the much larger ground-state absorption cross sections at 532 nm for **Ir-3** and **Ir-4** counter-played the excited-state absorption. Consequently, the RSA of **Ir-3** and **Ir-4** is weaker than their corresponding counterpart **Ir-1** and **Ir-2**. Between **Ir-3** and **Ir-4**, the stronger RSA of **Ir-3** should be attributed to its much

stronger excited-state absorption but weaker ground-state absorption at 532 nm compared to those of **Ir-4**, giving rise to larger $\sigma_{\text{ex}}/\sigma_0$ ratio for **Ir-3** than that for **Ir-4**. Considering the broader and stronger excited-state absorption at 500–800 nm and the weak ground-state absorption at 520–700 nm in **Ir-3**, **Ir-3** could potentially be a better broadband reverse saturable absorber.

4. Conclusions

We synthesized and investigated the photophysical properties and RSA of four cationic Ir(III) complexes bearing **quqo** core ligand, which were designed to improve the triplet excited-state absorption and prolong the triplet lifetime while red-shifting the weak charge transfer ground-state absorption band(s) to longer visible spectral regions. Both the experimental and TDDFT calculation results indicated that incorporation of the π -donating fluorenyl substituent to the **quqo** diimine ligand changed the nature of the lowest triplet state transitions of complexes **Ir-3** and **Ir-4** to the predominant diimine ligand-based $^3\pi, \pi^*/^3\text{ILCT}$ configurations, which is different from the dominant $^3\text{LLCT}/^3\text{MLCT}$ transitions for **T₁** in **Ir-1** and **Ir-2**. Such a change prolonged the triplet lifetimes of **Ir-3** and **Ir-4** and enhanced their excited-state absorption and emission efficiencies. In contrast, introducing larger π -conjugated cyclometalating C^N ligand **dppi** in **Ir-2** and **Ir-4** had little effect on the nature of their lowest triplet excited states in comparison to their corresponding counterpart **Ir-1** and **Ir-3**, except for that the emission spectrum of **Ir-2** was red-shifted with respect to that of **Ir-1**, and the TA signals of **Ir-4** were much weaker than those of **Ir-3**. All complexes exhibited reverse saturable absorption at 532 nm for ns laser pulses, with the RSA strength following the trend of **Ir-1** > **Ir-2** \approx **Ir-3** > **Ir-4**. The strongest RSA of **Ir-1** is attributed to its weakest ground-state absorption at 532 nm compared to the other three complexes. Although the excited-state absorption of **Ir-3** and **Ir-4** is stronger than those of **Ir-1** and **Ir-2** at 532 nm, their much stronger ground-state absorption counter-played the excited-state absorption and led to reduced RSA at 532 nm in **Ir-3** and **Ir-4** with respect to their counterpart **Ir-1** and **Ir-2**, respectively. However, considering the longer triplet lifetimes and broader and stronger triplet excited-state absorption of **Ir-3** and **Ir-4** at > 550 nm, we anticipate that these two complexes, especially **Ir-3**, have the potential to be used as broadband RSA materials.

CRedit authorship contribution statement

Hui Li: Methodology, Investigation, Validation, Visualization, Data curation, Writing - original draft. **Shan Liu:** Investigation. **Levi Lystrom:** Investigation, Visualization, Data curation, Writing - original draft. **Svetlana Kilina:** Resources, Writing - review & editing, Supervision, Funding acquisition. **Wenfeng Sun:** Conceptualization, Formal analysis, Resources, Writing - review & editing, Visualization, Data curation, Supervision, Project administration, Funding acquisition.

Declaration of Competing Interest

The authors declare that they have no known competing financial interests or personal relationships that could have appeared to influence the work reported in this paper.

Acknowledgements

The synthesis and photophysical studies of this work were supported by the Army Research Laboratory (W911NF-10-2-0055) to W. Sun. The DFT calculations were supported by the National Science Foundation (NSF DMR-1411086 and CHE-1800476) to W. Sun and S. Kilina. For computational resources and administrative support, we

thank the Center for Computationally Assisted Science and Technology (CCAST) at North Dakota State University.

Appendix A. Supplementary data

Supplementary material related to this article can be found, in the online version, at doi:<https://doi.org/10.1016/j.jphotochem.2020.112609>.

References

- [1] S. Lamansky, P. Djurovich, D. Murphy, F. Abdel-Razzaq, H.-E. Lee, C. Adachi, P.E. Burrows, S.R. Forrest, M.E. Thompson, Highly phosphorescent bis-cyclometalated iridium complexes: synthesis, photophysical characterization, and use in organic light emitting diodes, *J. Am. Chem. Soc.* 123 (2001) 4304–4312, <https://doi.org/10.1021/ja003693s>.
- [2] C. Ulbricht, B. Beyer, C. Friebe, A. Winter, U.S. Schubert, Recent developments in the application of phosphorescent iridium(III) complex systems, *Adv. Mater.* 21 (2009) 4418–4441, <https://doi.org/10.1002/adma.200803537>.
- [3] P. Pla, J.M. Junquera-Hernandez, H.J. Bolink, E. Orti, Emission energy of azole-based ionic iridium(III) complexes: a theoretical study, *Dalton Trans.* 44 (2015) 8497–8505, <https://doi.org/10.1039/c4dt03046j>.
- [4] Q.-L. Xu, X. Liang, L. Jiang, Y. Zhao, Y.-X. Zheng, Two blue iridium complexes for efficient electroluminescence with low efficiency roll-off, *RSC Adv.* 5 (2015) 89218–89225, <https://doi.org/10.1039/C5RA14837E>.
- [5] Q.-L. Xu, X. Liang, S. Zhang, Y.-M. Jing, X. Liu, G.-Z. Lu, Y.-X. Zheng, J.-L. Zuo, Efficient OLEDs with low efficiency roll-off using iridium complexes possessing good electron mobility, *J. Mater. Chem. C* 3 (2015) 3694–3701, <https://doi.org/10.1039/C5TC00073D>.
- [6] D. Tordera, S. Meier, M. Lenes, R.D. Costa, E. Orti, W. Sarfert, H.J. Bolink, Simple, fast, bright, and stable light sources, *Adv. Mater.* 24 (2012) 897–900, <https://doi.org/10.1002/adma.201104047>.
- [7] A.M. Bünzli, E.C. Constable, C.E. Housecroft, A. Prescimone, J.A. Zampese, G. Longo, L. Gil-Escrig, A. Pertegás, E. Orti, H.J. Bolink, Exceptionally long-lived light-emitting electrochemical cells: multiple intra-cation π -stacking interactions in $[\text{Ir}(\text{C}^{\text{N}})_2(\text{N}^{\text{N}})]\text{PF}_6$ emitters, *Chem. Sci.* 6 (2015) 2843–2852, <https://doi.org/10.1039/C4SC03942D>.
- [8] A.G. Condie, J.C. Gonzalez-Gomez, C.R. Stephenson, Visible-light photoredox catalysis: aza-henry reactions via C–H functionalization, *J. Am. Chem. Soc.* 132 (2010) 1464–1465, <https://doi.org/10.1021/ja909145y>.
- [9] J. Sun, J. Zhao, H. Guo, W. Wu, Visible-light harvesting iridium complexes as singlet oxygen sensitizers for photooxidation of 1,5-dihydroxynaphthalene, *Chem. Commun.* 48 (2012) 4169–4171, <https://doi.org/10.1039/C2CC16690A>.
- [10] X. Wang, J. Jia, Z. Huang, M. Zhou, H. Fei, Luminescent peptide labeling based on a histidine-binding iridium(III) complex for cell penetration and intracellular targeting studies, *Chem. Eur. J.* 17 (2011) 8028–8032, <https://doi.org/10.1002/chem.201100568>.
- [11] K.K.-W. Lo, K.Y. Zhang, Iridium(III) complexes as therapeutic and bioimaging reagents for cellular applications, *RSC Adv.* 2 (2012) 12069–12083, <https://doi.org/10.1039/C2RA20967E>.
- [12] C. Jin, J. Liu, Y. Chen, L. Zeng, R. Guan, C. Ouyang, L. Ji, H. Chao, Cyclometalated iridium(III) complexes as two-photon phosphorescent probes for specific mitochondrial dynamics tracking in living cells, *Chem. Eur. J.* 21 (2015) 12000–12010, <https://doi.org/10.1002/chem.201501882>.
- [13] H. Huang, B. Yu, P. Zhang, J. Huang, Y. Chen, G. Gasser, L. Ji, H. Chao, Highly charged ruthenium(II) polypyridyl complexes as lysosome-localized photosensitizers for two-photon photodynamic therapy, *Angew. Chem. Int. Ed.* 54 (2015) 14049–14052, <https://doi.org/10.1002/anie.201507800>.
- [14] W. Wang, Z. Mao, M. Wang, L.J. Liu, D.W. Kwong, C.H. Leung, D.L. Ma, A long lifetime luminescent iridium(III) complex chemosensor for the selective switch-on detection of Al^{3+} ions, *Chem. Commun.* 52 (2016) 3611–3614, <https://doi.org/10.1039/C5CC10383E>.
- [15] Y. You, S. Cho, W. Nam, Cyclometalated iridium(III) complexes for phosphorescence sensing of biological metal ions, *Inorg. Chem.* 53 (2014) 1804–1815, <https://doi.org/10.1021/ic4013872>.
- [16] A. Zamora, G. Viguera, V. Rodríguez, M.D. Santana, J. Ruiz, Cyclometalated iridium(III) luminescent complexes in therapy and phototherapy, *Coord. Chem. Rev.* 360 (2018) 34–76, <https://doi.org/10.1016/j.ccr.2018.01.010>.
- [17] C. Dragonetti, A. Colombo, D. Marinotto, S. Righetto, D. Roberto, A. Valore, M. Escadeillas, V. Guerschais, H. Le Bozec, A. Boucekkine, C. Latouche, Functionalized styryl iridium(III) complexes as active second-order NLO chromophores and building blocks for SHG polymeric films, *J. Organomet. Chem.* 751 (2014) 568–572, <https://doi.org/10.1016/j.jorganchem.2013.09.003>.
- [18] S. Fantacci, F. De Angelis, A computational approach to the electronic and optical properties of Ru(II) and Ir(III) polypyridyl complexes: applications to DSC, OLED and NLO, *Coord. Chem. Rev.* 255 (2011) 2704–2726, <https://doi.org/10.1016/j.ccr.2011.03.008>.
- [19] C. Dragonetti, S. Righetto, D. Roberto, R. Ugo, A. Valore, S. Fantacci, A. Sgamellotti, F. De Angelis, Cyclometalated iridium(III) complexes with substituted 1,10-phenanthrolines: a new class of highly active organometallic second order NLO-phores with excellent transparency with respect to second harmonic emission, *Chem. Commun.* (2007) 4116–4118, <https://doi.org/10.1039/B708073E>.
- [20] V. Aubert, L. Ordonneau, M. Escadeillas, J.A. Williams, A. Boucekkine, E. Coulaud, C. Dragonetti, S. Righetto, D. Roberto, R. Ugo, A. Valore, A. Singh, J. Zyss, I. Ledoux-Rak, H. Le Bozec, V. Guerschais, Linear and nonlinear optical properties of cationic bipyridyl iridium(III) complexes: tunable and photoswitchable? *Inorg. Chem.* 50 (2011) 5027–5038, <https://doi.org/10.1021/ic2002892>.
- [21] Y. You, W. Nam, Photofunctional triplet excited states of cyclometalated Ir(III) complexes: beyond electroluminescence, *Chem. Soc. Rev.* 41 (2012) 7061–7084, <https://doi.org/10.1039/C2CS35171D>.
- [22] K.Y. Kim, R.T. Farley, K.S. Schanze, An iridium(III) complex that exhibits dual mechanism nonlinear absorption, *J. Phys. Chem. B* 110 (2006) 17302–17304, <https://doi.org/10.1021/jp063916m>.
- [23] Y. Li, N. Dandu, R. Liu, L. Hu, S. Kilina, W. Sun, Nonlinear absorbing cationic iridium(III) complexes bearing benzothiazolylfluorene motif on the bipyridine (NAN) ligand: synthesis, photophysics and reverse saturable absorption, *ACS Appl. Mater. Interfaces* 5 (2013) 6556–6570, <https://doi.org/10.1021/am401133p>.
- [24] Z. Li, P. Cui, C. Wang, S. Kilina, W. Sun, Nonlinear absorbing cationic bipyridyl iridium(III) complexes bearing cyclometalating ligands with different degrees of π -conjugation: synthesis, photophysics, and reverse saturable absorption, *J. Phys. Chem. C* 118 (2014) 28764–28775, <https://doi.org/10.1021/jp5073457>.
- [25] R. Liu, N. Dandu, J. Chen, Y. Li, Z. Li, S. Liu, C. Wang, S. Kilina, B. Kohler, W. Sun, Influence of different diimine (N^{N}) ligands on the photophysics and reverse saturable absorption of heteroleptic cationic iridium(III) complexes bearing cyclometalating 2-{3-[7-(benzothiazol-2-yl)fluoren-2-yl]phenyl}pyridine (C^{N}) ligands, *J. Phys. Chem. C* 118 (2014) 23233–23246, <https://doi.org/10.1021/jp506765k>.
- [26] Y. Li, N. Dandu, R. Liu, Z. Li, S. Kilina, W. Sun, Effects of extended π -conjugation in phenanthroline (N^{N}) and phenylpyridine (C^{N}) ligands on the photophysics and reverse saturable absorption of cationic heteroleptic iridium(III) complexes, *J. Phys. Chem. C* 118 (2014) 6372–6384, <https://doi.org/10.1021/jp411259f>.
- [27] Y. Li, N. Dandu, R. Liu, S. Kilina, W. Sun, Synthesis and photophysics of reverse saturable absorbing heteroleptic iridium(III) complexes bearing 2-(7-R-fluoren-2'-yl)pyridine ligands, *Dalton Trans.* 43 (2014) 1724–1735, <https://doi.org/10.1039/C3DT52184B>.
- [28] T.M. Pritchett, M.J. Ferry, W.M. Shensky, A.G. Mott, D.J. Stewart, S.L. Long, J.E. Haley, Z. Li, W. Sun, Strong triplet excited-state absorption in a phenanthroline iridium(III) complex with benzothiazolylfluorenyl-substituted ligands, *Opt. Lett.* 40 (2015) 186–189, <https://doi.org/10.1364/OL.40.000186>.
- [29] C. Wang, L. Lystrom, H. Yin, M. Hetu, S. Kilina, S.A. McFarland, W. Sun, Increasing the triplet lifetime and extending the ground-state absorption of bis(cyclometalated Ir(III)) complexes for reverse saturable absorption and photodynamic therapy applications, *Dalton Trans.* 45 (2016) 16366–16378, <https://doi.org/10.1039/C6DT02416E>.
- [30] X. Zhu, L. Lystrom, S. Kilina, W. Sun, Tuning the photophysics and reverse saturable absorption of heteroleptic cationic iridium(III) complexes via substituents on the 6,6'-bis(flouren-2-yl)-2,2'-biquinoline ligand, *Inorg. Chem.* 55 (2016) 11908–11919, <https://doi.org/10.1021/acs.inorgchem.6b02028>.
- [31] R. Liu, N. Dandu, C. McCleese, Y. Li, T. Lu, H. Li, D. Yost, C. Wang, S. Kilina, C. Burda, W. Sun, Influence of a naphthaldiimide substituent at the diimine ligand on the photophysics and reverse saturable absorption of Pt^{II} diimine complexes and cationic Ir^{III} complexes, *Eur. J. Inorg. Chem.* Issue 31 (2015) 5241–5253, <https://doi.org/10.1002/ejic.201500882>.
- [32] C. Pei, P. Cui, C. McCleese, S. Kilina, C. Burda, W. Sun, Heteroleptic cationic iridium(III) complexes bearing naphthalimide substituents: synthesis, photophysics and reverse saturable absorption, *Dalton Trans.* 44 (2015) 2176–2190, <https://doi.org/10.1039/C4DT02384F>.
- [33] Z. Li, H. Li, B.J. Gifford, W.D.N. Peiris, S. Kilina, W. Sun, Synthesis, photophysics, and reverse saturable absorption of 7-(benzothiazol-2-yl)-9,9-di(2-ethylhexyl)-9H-fluoren-2-yl tethered $[\text{Ir}(\text{bpy})_2]\text{PF}_6$ and $[\text{Ir}(\text{ppy})_3]$ complexes (bpy = 2,2'-bipyridine, ppy = 2-phenylpyridine), *RSC Adv.* 6 (2016) 41214–41228, <https://doi.org/10.1039/C5RA20084A>.
- [34] W. Sun, C. Pei, T. Lu, P. Cui, Z. Li, C. McCleese, Y. Fang, S. Kilina, Y. Song, C. Burda, Reverse saturable absorbing cationic iridium(III) complexes bearing the 2-(2-quinolinyl)quinoxaline ligand: effects of different cyclometalating ligands on linear and nonlinear absorption, *J. Mater. Chem. C* 4 (2016) 5059–5072, <https://doi.org/10.1039/C6TC00710D>.
- [35] X. Zhu, P. Cui, S. Kilina, W. Sun, Multifunctional cationic iridium(III) complexes bearing 2-aryloxazolo[4,5-f][1,10]phenanthroline (N^{N}) ligand: synthesis, crystal structure, photophysics, mechanochromic/vapochromic effects, and reverse saturable absorption, *Inorg. Chem.* 56 (2017) 13715–13731, <https://doi.org/10.1021/acs.inorgchem.7b01472>.
- [36] L. Wang, P. Cui, S. Kilina, W. Sun, Toward broadband reverse saturable absorption: investigating the impact of cyclometalating ligand π -conjugation on the photophysics and reverse saturable absorption of cationic heteroleptic iridium complexes, *J. Phys. Chem. C* 121 (2017) 5719–5730, <https://doi.org/10.1021/acs.jpcc.6b12947>.
- [37] L. Wang, P. Cui, S. Kilina, W. Sun, Heteroleptic cationic iridium(III) complexes bearing phenanthroline derivatives with extended π -conjugation as potential broadband reverse saturable absorbers, *New J. Chem.* 44 (2020) 456–465, <https://doi.org/10.1039/C9NJ03877A>.
- [38] B. Liu, L. Lystrom, S.L. Brown, E.K. Hobbie, S. Kilina, W. Sun, Impact of benzanulation site at the diimine (N^{N}) ligand on the excited-state properties and reverse saturable absorption of bis(cyclometalated iridium(III)) complexes, *Inorg. Chem.* 58 (2019) 5483–5493, <https://doi.org/10.1021/acs.inorgchem.8b03162>.
- [39] B. Liu, L. Lystrom, C.G. Cameron, S. Kilina, S.A. McFarland, W. Sun, Monocationic iridium(III) complexes with far-red charge-transfer absorption and near-IR

- emission: synthesis, photophysics, and reverse saturable absorption, *Eur. J. Inorg. Chem.* Issue 16 (2019) 2208–2215, <https://doi.org/10.1002/ejic.201900156>.
- [40] B. Liu, L. Lystrom, S. Kilina, W. Sun, Effects of varying the benzannulation site and π conjugation of the cyclometalating ligand on the photophysics and reverse saturable absorption of monocationic iridium(III) complexes, *Inorg. Chem.* 58 (2019) 476–488, <https://doi.org/10.1021/acs.inorgchem.8b02714>.
- [41] I. Avilov, P. Minoofar, J. Cornil, L. De Cola, Influence of substituents on the energy and nature of the lowest excited states of heteroleptic phosphorescent Ir(III) complexes: a joint theoretical and experimental study, *J. Am. Chem. Soc.* 129 (2007) 8247–8258, <https://doi.org/10.1021/ja0711011>.
- [42] Q. Zhao, M. Yu, L. Shi, S. Liu, C. Li, M. Shi, Z. Zhou, C. Huang, F. Li, Cationic iridium(III) complexes with tunable emission color as phosphorescent dyes for live cell imaging, *Organometallics* 29 (2010) 1085–1091, <https://doi.org/10.1021/om900691r>.
- [43] S. Stagni, S. Colella, A. Palazzi, G. Valenti, S. Zacchini, F. Paolucci, M. Marcaccio, R.Q. Albuquerque, L. De Cola, Essential role of the ancillary ligand in the color tuning of iridium tetrazolate complexes, *Inorg. Chem.* 47 (2008) 10509–10521, <https://doi.org/10.1021/ic801157k>.
- [44] Y. You, S.Y. Park, Phosphorescent iridium(III) complexes: toward high phosphorescence quantum efficiency through ligand control, *Dalton Trans.* (2009) 1267–1282, <https://doi.org/10.1039/B812281D>.
- [45] C. Li, L. Zhang, R. Wang, Y. Song, Y. Wang, Dynamics of reverse saturable absorption and all-optical switching in C_{60} , *J. Opt. Soc. Am. B* 11 (1994) 1356–1360, <https://doi.org/10.1364/JOSAB.11.001356>.
- [46] A. Penzkofer, Passive Q-switching and mode-locking for the generation of nanosecond to femtosecond pulses, *Appl. Phys. B* 46 (1988) 43–46, <https://doi.org/10.1007/BF00698653>.
- [47] Y.B. Band, D. Harter, R. Bavli, Optical pulse compressor composed of saturable and reverse saturable absorbers, *Chem. Phys. Lett.* 126 (1986) 280–284, [https://doi.org/10.1016/S0009-2614\(86\)80083-5](https://doi.org/10.1016/S0009-2614(86)80083-5).
- [48] G.S. He, L.S. Tan, Q. Zheng, P.N. Prasad, Multiphoton absorbing materials: molecular designs, characterizations, and applications, *Chem. Rev.* 108 (2008) 1245–1330, <https://doi.org/10.1021/cr050054x>.
- [49] A.B. Tamayo, S. Garon, T. Sajoto, P.I. Djurovich, I.M. Tsyba, R. Bau, M.E. Thompson, Cationic bis-cyclometalated iridium(III) diimine complexes and their use in efficient blue, green, and red electroluminescent devices, *Inorg. Chem.* 44 (2005) 8723–8732, <https://doi.org/10.1021/ic050970t>.
- [50] F. De Angelis, S. Fantacci, N. Evans, C. Klein, S.M. Zakeeruddin, J.E. Moser, K. Kalyanasundaram, H.J. Bolink, M. Gratzel, M.K. Nazeeruddin, Controlling phosphorescence color and quantum yields in cationic iridium complexes: a combined experimental and theoretical study, *Inorg. Chem.* 46 (2007) 5989–6001, <https://doi.org/10.1021/ic700435c>.
- [51] M.S. Lowry, S. Bernhard, Synthetically tailored excited states: phosphorescent, cyclometalated iridium(III) complexes and their applications, *Chem. Eur. J.* 12 (2006) 7970–7977, <https://doi.org/10.1002/chem.200600618>.
- [52] C. Dragonetti, S. Righetto, D. Roberto, A. Valore, T. Benincori, F. Sannicolò, F. De Angelis, S. Fantacci, Cationic cyclometalated iridium(III) complexes with substituted 1,10-phenanthrolines: the role of the cyclometalated moiety on this new class of complexes with interesting luminescent and second order non linear optical properties, *J. Mater. Sci. Mater. Electron.* 20 (2009) 460–464, <https://doi.org/10.1007/s10854-008-9670-9>.
- [53] M.S. Lowry, W.R. Hudson, R.A. Pascal, S. Bernhard, Accelerated luminophore discovery through combinatorial synthesis, *J. Am. Chem. Soc.* 126 (2004) 14129–14135, <https://doi.org/10.1021/ja047156+>.
- [54] C. Dragonetti, L. Falcioni, P. Mussini, S. Righetto, D. Roberto, R. Ugo, A. Valore, F. De Angelis, S. Fantacci, A. Sgamellotti, M. Ramon, M. Muccini, The role of substituents on functionalized 1,10-phenanthroline in controlling the emission properties of cationic iridium(III) complexes of interest for electroluminescent devices, *Inorg. Chem.* 46 (2007) 8533–8547, <https://doi.org/10.1021/ic700414z>.
- [55] C.-H. Yang, M. Mauro, F. Polo, S. Watanabe, I. Muenster, R. Fröhlich, L.D. Cola, Deep-blue-emitting heteroleptic iridium(III) complexes suited for highly efficient phosphorescent OLEDs, *Chem. Mater.* 24 (2012) 3684–3695, <https://doi.org/10.1021/cm3010453>.
- [56] K.S. Bejomyandhas, A. Kumar, S. Varughese, E. Varathan, V. Subramanian, M.L.P. Reddy, Photophysical and electroluminescence properties of bis(2',6'-difluoro-2,3'-bipyridinato-*N*,*C*4')iridium(picolinate) complexes: effect of electron-withdrawing and electron-donating group substituents at the 4' position of the pyridyl moiety of the cyclometalated ligand, *J. Mater. Chem. C* 3 (2015) 7405–7420, <https://doi.org/10.1039/C5TC01260K>.
- [57] Q. Zhao, S. Liu, M. Shi, C. Wang, M. Yu, L. Li, F. Li, T. Yi, C. Huang, Series of new cationic iridium(III) complexes with tunable emission wavelength and excited state properties: structures, theoretical calculations, and photophysical and electrochemical properties, *Inorg. Chem.* 45 (2006) 6152–6160, <https://doi.org/10.1021/ic052034j>.
- [58] B. Liu, L. Lystrom, S. Kilina, W. Sun, Tuning the ground state and excited state properties of monocationic iridium(III) complexes by varying the site of benzannulation on diimine ligand, *Inorg. Chem.* 56 (2017) 5361–5370, <https://doi.org/10.1021/acs.inorgchem.7b00467>.
- [59] G. Le Douaron, F. Schmidt, M. Amar, H. Kadar, L. Debortoli, A. Latini, B. Seon-Meniel, L. Ferrie, P.P. Michel, D. Touboul, A. Brunelle, R. Raisman-Vozari, B. Figadere, Neuroprotective effects of a brain permeant 6-aminoquinoline derivative in cell culture conditions that model the loss of dopaminergic neurons in Parkinson disease, *Eur. J. Med. Chem.* 89 (2015) 467–479, <https://doi.org/10.1016/j.ejmech.2014.10.067>.
- [60] R.B.P. Elmes, M. Erby, S.M. Cloonan, S.J. Quinn, D.C. Williams, T. Gunnlaugsson, Quaternized pdppz: synthesis, DNA-binding and biological studies of a novel dppz derivative that causes cellular death upon light irradiation, *Chem. Commun.* 47 (2011) 686–688, <https://doi.org/10.1039/C0CC04303F>.
- [61] J. Jo, C. Chi, S. Hoyer, G. Wegner, D.Y. Yoon, Synthesis and characterization of monodisperse oligofluorenes, *Chem. Eur. J.* 10 (2004) 2681–2688, <https://doi.org/10.1002/chem.200305659>.
- [62] T. Linder, E. Badiola, T. Baumgartner, T.C. Sutherland, Synthesis of π -extended thiadiazole (oxides) and their electronic properties, *Org. Lett.* 12 (2010) 4520–4523, <https://doi.org/10.1021/ol1018213>.
- [63] X. Yi, P. Yang, D. Huang, J. Zhao, Visible light-harvesting cyclometalated Ir(III) complexes with pyreno[4,5-*d*]imidazole C'*N* ligands as triplet photosensitizers for triplet-triplet annihilation upconversion, *Dyes Pigm.* 96 (2013) 104–115, <https://doi.org/10.1016/j.dyepig.2012.07.020>.
- [64] Y. Yuan, D. Li, X. Zhang, X. Zhao, Y. Liu, J. Zhang, Y. Wang, Phenanthroimidazole-derivative semiconductors as functional layer in high performance OLEDs, *New J. Chem.* 35 (2011) 1534–1540, <https://doi.org/10.1039/C1NJ20072K>.
- [65] A.B. Tamayo, B.D. Alleyne, P.I. Djurovich, S. Lamansky, I. Tsyba, N.N. Ho, R. Bau, M.E. Thompson, Synthesis and characterization of facial and meridional tris-cyclometalated iridium(III) complexes, *J. Am. Chem. Soc.* 125 (2003) 7377–7387, <https://doi.org/10.1021/ja034537z>.
- [66] J.N. Demas, G.A. Crosby, The measurement of photoluminescence quantum yields. A review, *J. Phys. Chem.* 75 (1971) 991–1024, <https://doi.org/10.1021/j100678a001>.
- [67] K. Suzuki, A. Kobayashi, S. Kaneko, K. Takehira, T. Yoshihara, H. Ishida, Y. Shiina, S. Oishi, S. Tobita, Reevaluation of absolute luminescence quantum yields of standard solutions using a spectrometer with an integrating sphere and a back-thinned CCD detector, *Phys. Chem. Chem. Phys.* 11 (2009) 9850–9860, <https://doi.org/10.1039/B912178A>.
- [68] W.H. Melhuish, Quantum efficiencies of fluorescence of organic substances: effect of solvent and concentration of the fluorescent solute, *J. Phys. Chem.* 65 (1961) 229–235, <https://doi.org/10.1021/j100820a009>.
- [69] W. Sun, H. Zhu, P.M. Barron, Binuclear cyclometalated platinum(II) 4,6-diphenyl-2,2'-bipyridine complexes: interesting photoluminescent and optical limiting materials, *Chem. Mater.* 18 (2006) 2602–2610, <https://doi.org/10.1021/cm060161n>.
- [70] F. Guo, W. Sun, Y. Liu, K. Schanze, Synthesis, photophysics, and optical limiting of platinum(II) 4'-tolylterpyridyl arylacetylde complexes, *Inorg. Chem.* 44 (2005) 4055–4065, <https://doi.org/10.1021/ic049266n>.
- [71] M.J. Frisch, G.W. Trucks, H.B. Schlegel, G.E. Scuseria, M.A. Robb, J.R. Cheeseman, G. Scalmani, V. Barone, B. Mennucci, G.A. Petersson, H. Nakatsuji, M. Caricato, X. Li, H.P. Hratchian, A.F. Izmaylov, J. Bloino, G. Zheng, J.L. Sonnenberg, M. Hada, M. Ehara, K. Toyota, R. Fukuda, J. Hasegawa, M. Ishida, T. Nakajima, Y. Honda, O. Kitao, H. Nakai, T. Vreven, J.J.A. Montgomery, J.E. Peralta, F. Ogliaro, M. Bearpark, J.J. Heyd, E. Brothers, K.N. Kudin, V.N. Staroverov, R. Kobayashi, J. Normand, K. Raghavachari, A. Rendell, J.C. Burant, S.S. Iyengar, J. Tomasi, M. Cossi, N. Rega, N.J. Millam, M. Klene, J.E. Knox, J.B. Cross, V. Bakken, C. Adamo, J. Jaramillo, R. Gomperts, R.E. Stratmann, O. Yazyev, A.J. Austin, R. Cammi, C. Pomelli, J.W. Ochterski, R.L. Martin, K. Morokuma, V.G. Zakrzewski, G.A. Voth, P. Salvador, J.J. Dannenberg, S. Dapprich, A.D. Daniels, Ö. Farkas, J.B. Foresman, J.V. Ortiz, J. Cioslowski, D.J. Fox, Gaussian 09, Revision A.1, Gaussian Inc., Wallingford, CT, USA, 2009.
- [72] M. Cossi, V. Barone, R. Cammi, J. Tomasi, Ab initio study of solvated molecules: a new implementation of the polarizable continuum model, *Chem. Phys. Lett.* 255 (1996) 327–335, [https://doi.org/10.1016/0009-2614\(96\)00349-1](https://doi.org/10.1016/0009-2614(96)00349-1).
- [73] V. Barone, M. Cossi, J. Tomasi, Geometry optimization of molecular structures in solution by the polarizable continuum model, *J. Comput. Chem.* 19 (1998) 404–417, [https://doi.org/10.1002/\(SICI\)1096-987X\(199803\)19:4<404::AID-JCC3>3.0.CO;2-W](https://doi.org/10.1002/(SICI)1096-987X(199803)19:4<404::AID-JCC3>3.0.CO;2-W).
- [74] J.P. Perdew, K. Burke, M. Ernzerhof, Generalized gradient approximation made simple, *Phys. Rev. Lett.* 77 (1996) 3865–3868, <https://doi.org/10.1103/PhysRevLett.77.3865>.
- [75] P.J. Hay, W.R. Wadt, Ab initio effective core potentials for molecular calculations. Potentials for the transition metal atoms Sc to Hg, *J. Chem. Phys.* 82 (1985) 270–283, <https://doi.org/10.1063/1.448799>.
- [76] P.J. Hay, W.R. Wadt, Ab initio effective core potentials for molecular calculations. Potentials for K to Au including the outermost core orbitals, *J. Chem. Phys.* 82 (1985) 299–310, <https://doi.org/10.1063/1.448975>.
- [77] R. Krishnan, J.S. Binkley, R. Seeger, J.A. Pople, Self-consistent molecular orbital methods. XX. A basis set for correlated wave functions, *J. Chem. Phys.* 72 (1980) 650–654, <https://doi.org/10.1063/1.438955>.
- [78] P.C. Hariharan, J.A. Pople, The influence of polarization functions on molecular orbital hydrogenation energies, *Theor. Chim. Acta* 28 (1973) 213–222, <https://doi.org/10.1007/BF00533485>.
- [79] T. Clark, J. Chandrasekhar, G.W. Spitznagel, P.V.R. Schleyer, Efficient diffuse function-augmented basis sets for anion calculations. III. The 3-21 + G basis set for first-row elements, Li–F, *J. Comput. Chem.* 4 (1983) 294–301, <https://doi.org/10.1002/jcc.540040303>.
- [80] M.M. Francel, W.J. Pietro, W.J. Hehre, J.S. Binkley, M.S. Gordon, D.J. DeFrees, J.A. Pople, Self-consistent molecular orbital methods. XXIII. A polarization-type basis set for second-row elements, *J. Chem. Phys.* 77 (1982) 3654–3665, <https://doi.org/10.1063/1.444267>.
- [81] P.M.W. Gill, B.G. Johnson, J.A. Pople, M.J. Frisch, The performance of the Becke-Lee-Yang-Parr (B-LYP) density functional theory with various basis sets, *Chem. Phys. Lett.* 197 (1992) 499–505, [https://doi.org/10.1016/0009-2614\(92\)85807-M](https://doi.org/10.1016/0009-2614(92)85807-M).
- [82] S. Kilina, D. Kilin, S. Tretiak, Light-driven and phonon-assisted dynamics in organic and semiconductor nanostructures, *Chem. Rev.* 18 (2015) 5929–5978,

- <https://doi.org/10.1021/acs.chemrev.5b00012>.
- [83] R. Peverati, D.G. Truhlar, Quest for a universal density functional: the accuracy of density functionals across a broad spectrum of databases in chemistry and physics, *Philos. Trans. Math. Phys. Eng. Sci.* 372 (2014), <https://doi.org/10.1098/rsta.2012.0476> 20120476.
- [84] S.-C. Qi, J.-i. Hayashi, L. Zhang, Recent application of calculations of metal complexes based on density functional theory, *RSC Adv.* 6 (2016) 77375–77395 <https://pubs.rsc.org/en/content/articlehtml/2016/ra/c6ra16168e>.
- [85] K.I. Igumenshchev, S. Tretiak, V.Y. Chernyak, Excitonic effects in a time-dependent density functional theory, *J. Chem. Phys.* 127 (2007) 127–136, <https://doi.org/10.1063/1.2773727>.
- [86] T. Lu, C. Wang, L. Lystrom, C. Pei, S. Kilina, W. Sun, Effects of extending the π -conjugation of the acetylide ligand on the photophysics and reverse saturable absorption of Pt(II) bipyridine bisacetylide complexes, *Phys. Chem. Chem. Phys.* 18 (2016) 28674–28687, <https://doi.org/10.1039/C6CP02628A>.
- [87] T.M. Henderson, A.F. Izmaylov, G. Scalmani, G.E. Scuseria, Can short-range hybrids describe long-range-dependent properties? *J. Chem. Phys.* 131 (2009) 044108–044117, <https://doi.org/10.1063/1.3185673>.
- [88] J.-D. Chai, M. Head-Gordon, Long-range corrected hybrid density functionals with damped atom-atom dispersion corrections, *Phys. Chem. Chem. Phys.* 20 (2008) 6615–6620, <https://doi.org/10.1039/B810189B>.
- [89] R.L. Martin, Natural transition orbitals, *J. Chem. Phys.* 118 (2003) 4775–4777, <https://doi.org/10.1063/1.1558471>.
- [90] R. Dennington, Inc.: Shawnee Mission, KS, (2007).
- [91] J.P. Perdew, M. Ernzerhof, K. Burke, Rationale for mixing exact exchange with density functional approximations, *J. Chem. Phys.* 105 (1996) 9982–9985, <https://doi.org/10.1063/1.472933>.
- [92] B. Liu, L. Lystrom, S. Kilina, W. Sun, Tuning the ground state and excited state properties of monocationic iridium(III) complexes by varying the site of benzanulation on diimine ligand, *Inorg. Chem.* 56 (2017) 5361–5370, <https://doi.org/10.1021/acs.inorgchem.7b00467>.
- [93] D.L. Ashford, C.R. Glasson, M.R. Norris, J.J. Concepcion, S. Keinan, M.K. Brennaman, J.L. Templeton, T.J. Meyer, Controlling ground and excited state properties through ligand changes in ruthenium polypyridyl complexes, *Inorg. Chem.* 53 (2014) 5637–5646, <https://doi.org/10.1021/ic500408j>.
- [94] X. Hui, J. Desrivot, C. Bories, P.M. Loiseau, X. Franck, R. Hocquemiller, B. Figadere, Synthesis and antiprotozoal activity of some new synthetic substituted quinoxalines, *Bioorg. Med. Chem. Lett.* 16 (2006) 815–820, <https://doi.org/10.1016/j.bmcl.2005.11.025>.
- [95] R. BÜRLI, A. F. Haugan, S. R. Mack, B. G. Perry, G. Raphy, E. A. Saville-Stones, Preparation of fused pyrazines as phosphoinositide 3-kinase (PI3K) inhibitors, Patent WO2010052448, 2010.
- [96] D. Roche, K. Prasad, O. Repic, T.J. Blacklock, Mild and regioselective oxidative bromination of anilines using potassium bromide and sodium perborate, *Tetrahedron Lett.* 41 (2000) 2083–2085, [https://doi.org/10.1016/S0040-4039\(00\)00119-2](https://doi.org/10.1016/S0040-4039(00)00119-2).
- [97] M.A.K. Zarchi, S.Z. Mousavi, Diazotization-bromination of aromatic amines using polymer-supported bromide via Sandmeyer-type reaction, *J. Polym. Res.* 21 (2014) 1–9, <https://doi.org/10.1007/s10965-013-0330-2>.
- [98] I. Beletskaya, A. Sigeev, A. Peregodov, P. Petrovskii, Catalytic sandmeyer bromination, *Synthesis* 16 (2007) 2534–2538, <https://doi.org/10.1055/s-2007-983784>.
- [99] L. Liu, Process for preparation of 3-halophenanthrenes from 3-aminophenanthrene, CN, 102101819 A (2011).
- [100] W. Wang, Process for the preparation of 5-bromophthalide, CN 1634906 A (2005).
- [101] L. T. Nagy, A. P. Behr, Z. Kapui, P. Aranyi, S. Batori, V. B. Bodor, M. Varga, G. Ferenczy, E. Mikus, K. Urban-Szabo, J. V. Szeredi, T. Szabo, E. Walcz, Preparation of (arylthio)acetamides and their S-oxides as CC chemokine receptor 3(CCR3) ligands, Patent WO2007034251, 2007.
- [102] E.C. Stokes, E.E. Langdon-Jones, L.M. Groves, J.A. Platts, P.N. Horton, I.A. Fallis, S.J. Coles, S.J. Pope, Cationic, luminescent cyclometalated iridium(III) complexes based on substituted 2-phenylthiazole ligands, *Dalton Trans.* 44 (2015) 8488–8496, <https://doi.org/10.1039/C4DT03054K>.
- [103] S. Lamansky, P. Djurovich, D. Murphy, F. Abdel-Razzaq, R. Kwong, I. Tsyba, M. Bortz, B. Mui, R. Bau, M.E. Thompson, Synthesis and characterization of phosphorescent cyclometalated iridium complexes, *Inorg. Chem.* 40 (2001) 1704–1711, <https://doi.org/10.1021/ic0008969>.
- [104] L. Flamigni, A. Barbieri, C. Sabatini, B. Ventura, F. Barigelli, Photochemistry and photophysics of coordination compounds: iridium, *Top. Curr. Chem.* 281 (2007) 143–203, https://doi.org/10.1007/128_2007_131.
- [105] K. Hasan, A.K. Bansal, I.D.W. Samuel, C. Roldan-Carmona, H.J. Bolink, E. Zysman-Colman, Tuning the emission of cationic iridium(III) complexes towards the red through methoxy substitution of the cyclometalating ligand, *Sci. Rep.* 5 (2015) 12325, <https://doi.org/10.1038/srep12325>.